

Multi-point Aerial Delivery System

A Major Qualifying Project Report

submitted to the faculty of the

WORCESTER POLYTECHNIC INSTITUTE

in Partial Fulfilment of the Requirements of the

Bachelor of Science Degree

in Aerospace Engineering

by

Johnathan Lazo

Johnathan Lazo

Trevor Shrady

Trevor Shrady

Anthony Gosselin

Anthony Gosselin

Benjamin English

Benjamin English

April 25, 2022

Approved by:

R. Cowlagi

Raghvendra V. Cowlagi, Advisor

Associate Professor, Aerospace Engineering Department, WPI.

Abstract

The goal of this project is to design and build a small-scale prototype of an autonomous multi-point aerial delivery vehicle with the goal of delivering payloads of 100-250 kg over ranges of 200-500 km. To this end, a fixed wing aircraft with wingspan 10 m and length 8.6 m is designed by modifying an existing aircraft design for similar purposes. Construction of a 1:10 scale prototype of the designed aircraft is reported. Detailed drawings of this prototype are provided. Preliminary results on the prototype construction, electronics assembly, and glide test are reported.

Fair use disclaimer:

This document may contain copyrighted material, such as photographs and diagrams, the use of which may not always have been specifically authorized by the copyright owner. The use of copyrighted material in this document is in accordance with the “fair use doctrine”, as incorporated in Title 17 USC §107 of the United States Copyright Act of 1976. This document is distributed without profit for educational purposes to those who have expressed interest in receiving the included information.

Acknowledgements

We would like to thank Professor Raghendra V. Cowlagi and Dr. Gregory Noetscher for their advice and guidance during this project. BRE would like to thank Abudula Aihaitjiang for his help with troubleshooting electronics and software issues throughout the project. We also would like to thank Worcester Polytechnic Institute and the US Army Combat Capabilities Development Command Soldier Center for their sponsorship and resources for the completion of this project.

Table of Contents

Abstract	2
Acknowledgements	4
Table of Figures	6
Table of Tables	10
Table of Authorship.....	11
1 Project Overview.....	13
1.1 Project Objectives	13
1.2 Literature Review	13
1.2.1 Current and Future Use of Airdrops in the Military:	13
1.2.2 History of Airdrops in the Army	14
1.2.3 Joint Precision Airdrop System (JPADS).....	14
1.2.4 UAVs and JPADS	14
1.2.5 Current UAV usage in the world	15
1.3 Design Requirements, Constraints, and Other Considerations	16
1.4 Project Management.....	16
1.4.1 Tasks and Timetable.....	16
1.5 Relevant Engineering Standards.....	18
1.6 Methods	18
1.7 Broader Impacts	19
2 System Design	22
2.1 Final Physical Design.....	22
2.2 Final Electronics.....	27
2.3 Conceptual Deployment Method.....	29
3 Design Process and Analysis.....	30
3.1 SolidWorks Modeling	30

3.1.1	Design Process of Fixed-Wing	32
	Weight Analysis of Design.....	34
3.1.2	34
3.1.3	Individual Parts of Model.....	38
	Construction Process	47
3.2	47
3.3	Electronics Process.....	55
4	Results.....	65
4.1	Numerical Simulation Results	65
4.2	Experimental Results.....	65
5	Conclusions.....	67
5.1	Recommendations for Future Work	67
	References	70
6	Appendix.....	72
6.1	Appendix 1: Drop Location MATLAB Code.....	72
6.2	Appendix 2: Glide Test Data MATLAB Code	75
6.3	Appendix 3: L/D Curves MATLAB Code	87
6.4	Appendix 4: Rate of Turn MATLAB Code.....	89
6.5	Appendix 5: Rate of climb MATLAB Code.....	90
6.6	Appendix 6: Air Density from Altitude MATLAB Code	90

Table of Figures

Figure 1:	Gantt Chart for A Term	16
Figure 2:	Gantt Chart for B Term	17
Figure 3:	Gantt Chart for C Term	17

Figure 4: Gantt Chart for D Term	18
<i>Figure 5: Completed Sub-Scale Build</i>	22
Figure 6: Final Fuselage Design	23
Figure 7: Close-up of Left Wing.....	24
Figure 8: Up-close View of Gap between “Control Surface” Ribs and Aileron (CAD).....	25
Figure 9: Top View of Wing Mount	25
Figure 10: Bottom View of Wing Mount.....	26
Figure 11: Empennage Assembly	26
Figure 12: Home Screen of Ardupilot Mission Planner	28
Figure 13: Sample Planned Mission in Mission Planner.....	29
Figure 14: Previous Fixed Wing Design.....	31
Figure 15: New Fixed Wing Design	31
Figure 16: Detailed Model of Sub-Scale.....	32
Figure 17: The Redesigned Fuselage	33
Figure 18: Shell of Fuselage	33
Figure 19: Mass Properties Estimation of Fuselage	34
Figure 20: Detailed Model of Sub-Scale.....	36
Figure 21: Initial Assembly of Sub-Scale Fuselage	39
Figure 22: Final Nosecone Model.....	40
Figure 23: Printed Nosecone.....	40
Figure 24: Wing Assembly Model.....	41
Figure 25: CAD for Full-Length Rib	41
Figure 26: CAD for Control Surface Rib	41
Figure 27: CAD for Control Adjacent Rib.....	42
Figure 28: Wing Mount Model.....	42
Figure 29: Aileron Model	43

Figure 30: Tail CAD Assembly	43
Figure 31: Model of Tail Mount	44
Figure 32: Dropping Mechanism Prototype.....	45
Figure 33: Rough Model of the Dropping Mechanism	46
Figure 34: 3-2-3 Stack of Foam Board (Uncut)	47
Figure 35: Using a weight and metal plate to ensure the hot glue adhered properly	47
Figure 36: Foam board cut to the width needed for the fuselage.....	48
Figure 37: Side view of cut foam board.....	48
Figure 38: Face of the cut foam board, scored to see necessary shape and dimensions of the resulting cylinder.....	48
Figure 39: Front view of the foam during cutting process	48
Figure 40: Top-down view of the foam board cut and shaped	49
Figure 41: Finished foam board fuselage.....	49
Figure 42: Laser Cut Fuselage and Wing ribs.....	49
Figure 43: Laser Cutting Tail Pathing.....	50
Figure 44: Laser Cutting Tail.....	50
Figure 45: 3D Printed Wing and Tail Mounts.....	51
Figure 46: 3D Printed Tail Control Surfaces.....	51
Figure 47: 3D Printed Nose Cone with Motor	52
Figure 48: 3D Printed Ailerons.....	52
Figure 49: Partially Assembled Fuselage.....	54
Figure 50: Process for Adding Ribs	54
Figure 51: Fuselage with Monokote	54
Figure 52: Final Aircraft.....	54
Figure 53: View of a Designed Mission on QGroundControl.....	55
Figure 54: Waypoint Customization in QGroundControl	56

Figure 55: Landing Pattern Customization in QGroundControl 57

Figure 56: Airframe and Port Assignments for the Model Aircraft..... 58

Figure 57: Example Wiring Diagram for Connecting a Servo and Motor to the PMB..... 59

Figure 58: The L/D Curve of the Full Scale..... 61

Figure 59: L/D Curve of the Sub Scale 62

Figure 60: Projectile Motion Plot for Payload Drop 65

Table of Tables

Table 1: Methods Used for Project Completion.....	18
Table 2: Mass estimations of full scale	34
Table 3: Mass estimations of the Subscale model.....	35
Table 4: The mass breakdown of the sub scale model	36
Table 5: Center of Mass after Payload Drops	37
Table 6: Pixhawk to PMB Wiring Ports	60

Table of Authorship

Section	Project Work	Report Writing
1. Project Overview	All	BRE
1.1. Project Objectives	All	TAS
1.2. Literature Review	All	BRE
1.3. Design Requirements	All	TAS
1.4. Project Management	All	TAS
1.5. Relevant Engineering Standards	All	BRE, TAS
1.6. Methods	All	All
1.7 Broader Impacts	BRE	BRE
2. System Design	All	All
2.1. Final Physical Design	JBL, TAS, APG	JBL, TAS
2.2. Final Electronics	BRE, APG	BRE
3. Design Process and Analysis	JBL, TAS	JBL
3.1. Design Process of Fixed-Wing	JBL, TAS	JBL, TAS
3.2. Construction Process	APG, TAS, JBL	JBL, APG
3.3. Electronics Process	BRE	BRE

3.4 Aerodynamic Performance Analysis	JBL	JBL
4. Results	All	All
4.1. Numerical Simulation Results	BRE	BRE
4.2. Experimental Results	All	BRE, TAS
5. Conclusions	N/A	All
5.1. Recommendations for Future Work	N/A	All

1 Project Overview

The United States Army has the need to deliver food, ammunition, and medical supplies to forward deployed soldiers who are on mission and unable to get back to a Forward Operating Base (FOB) to get resupplied. To serve this need, the objective of this project is to increase the range and payload capacity of current autonomous aerial delivery vehicles. The projected outcome of this project will enable the Army to resupply soldiers rapidly and reliably with a large number of supplies to continually keep soldiers fully equipped on the battlefield to keep their readiness and lethality up while on the battlefield. Our project specifically includes the designing of a full-scale model for the United States Army to use, in addition to the design and creation of a fully functioning subscale prototype, as a proof of concept of our design and of the project merits.

1.1 Project Objectives

The goal of this project is to design a full-scale autonomous fixed-wing aircraft that can make multiple (more than 3) payload drops with a Circular Error Probably (CEP) range of 10m. The target payload mass range is 100-250 kg of total payload. Another goal of this project is to build a sub-scale model to test flight dynamics and execute autonomous deliveries.

1.2 Literature Review

1.2.1 Current and Future Use of Airdrops in the Military:

In 2015 the army announced the “Force 2025 and Beyond” (F2025B) which is “the Army’s comprehensive strategy to change and deliver land-power capabilities as a strategic instrument of the future Joint Force.” The intellectual foundation for F2025B is “Win in a Complex World”, the U.S. Army Operating Concept [1].

As a part of the F2025B initiative, the Army is looking to enable autonomous aerial resupply within its brigade combat team (BCT). Autonomous delivery systems will be key a component at the tactical and operational levels. Supply convoys in Iraq and Afghanistan required manned aerial backup, while doing the missions autonomously would also free up the resources to either cut costs or redistribute the resources elsewhere, like in combat for example. Utilizing autonomous delivery will reduce manned cargo airlifts as well as ground vehicle convoys. Reducing manned delivery reduces risk exposure, extends operational reach, decrease customer wait time through point-to-point delivery (Like our project), and can increases delivery frequency [2].

1.2.2 History of Airdrops in the Army

The United States army has a long history of utilizing airdrop technology for both weaponry as well as supplying their troops on the battlefield. These airdrops were heavily utilized during World War II, with the United States dropping equipment, vehicles, and bombs. The U.S. also relied heavily on airdrops in Vietnam to resupply troops as they defended cities from the Vietcong. In more recent history, the Army airdropped supplies to their bases in Afghanistan to reduce the threat of explosive devices on the ground harming delivery vehicles. In addition to directly supplying their troops, the United States has also used airdrops to supply allies that could not receive supplies from their own countries. An example of this comes from World War II when the United States assisted Great Britain by airdropping supplies to Burma, Japan, behind Japanese lines [3].

1.2.3 Joint Precision Airdrop System (JPADS)

The United States Army currently uses JPADS to deliver cargo to forces from the air. JPADS uses a guidance system and parachute to deliver payloads to a target on a predetermined trajectory. JPADS allows for timely and accurate deliveries of crucial supplies while keeping soldiers safe from the dangers of traveling on the ground [4]. To determine the location of the airdrop, the US Army uses a mission planner named JPADS-MP. This mission planner uses high fidelity models of many factors to determine the drop location. The JPADS-MP uses a rugged laptop to perform its analysis and has the capabilities to receive information from aircraft that could assist in modeling. JPADS-MP can use either data pre-determined on the ground, or it can use data from the aircraft while it is in flight [5].

1.2.4 UAVs and JPADS

Utilizing autonomous aircraft and integrating the JPADS-MP system has the potential to expand the usefulness of both technologies. Since JPADS-MP can receive data from an aircraft, the Army could utilize that technology on an autonomous vehicle. Combining these technologies will enable the Army to continue delivering cargo at high accuracy while also keeping their troops out of potential danger while being in an aircraft around hostile territory [7] [8].

1.2.5 Current UAV usage in the world

Another aspect of the project is to utilize Unmanned Aerial Vehicles (UAVs). Some UAVs are currently used for delivery purposes, and one example of this was studied in Istanbul, Turkey at the beginning of the COVID-19 pandemic. In a study by Ozkan and Atli, they discussed how UAVs can be an integral step in healthcare logistics and supply chain networks. The UAV's utilized advantages over ground transportation such as no traffic and low overhead costs. Another large advantage that using a UAV had been the ability to reach places without accessible roads. The previous data showed that test results from 33 different test types that were flown to the laboratory were not different from their counterparts that utilized ground transportation. The paper concluded with a mathematical model on the most optimal trajectory and suggested that utilizing these UAVs could enable healthcare to reach farther distances throughout the nation. They could allow for faster times in transporting tests to the laboratories, making for faster turnaround time when receiving results [6].

1.3 Design Requirements, Constraints, and Other Considerations

Our given design requirements are that the aircraft be able to perform drops at multiple points during one mission, have a range of 200-500 kilometers and a total payload capacity of 100-250 kilograms. Additionally, the aircraft must be unmanned, autonomous, and be able to have the preloaded flight plan altered mid mission to account for mission variables changing.

1.4 Project Management

1.4.1 Tasks and Timetable

Actual work in A Term (8/25/2021 - 10/13/2021) progressed for the most part fairly similar to the schedule presented in the respective Gantt chart. There were a few minor setbacks due to having to regroup and reattack brainstorming the actual design of the aircraft; at first the team was looking to design a completely new airframe rather than utilize the one investigated by the previous year’s project team. These ideas, however, were reevaluated and were discarded in favor of a design relying on the data already available from the previous team’s work.

Task	Week 1	Week 2	Week 3	Week 4	Week 5	Week 6	Week 7
Project Scope							
Create Timeline							
SESA Trainings							
Literature Review							
Formulate Preliminary Direction of Project							
Research Fixed Wing Designs							
Solidworks Modelling							

Figure 1: Gantt Chart for A Term

In B Term (10/25/2021 - 12/16/2021), there were several major setbacks. After modelling the approximate payload size and shape it was determined that the fuselage geometry needed to be altered to allow for more space for internals. There were also delays in modelling of the subscale wing due to SolidWorks issues which took longer than expected to overcome.



Figure 2: Gantt Chart for B Term

C Term (1/12/2022 - 3/4/2022) saw its share of significant obstacles as well. At the end of week 3, it was decided to change the design of the fuselage entirely, switching from the original Styrofoam insulation sheet construction to a hollow, ribbed, balsa wood construction. This meant the CAD for the fuselage had to be redone almost from scratch, which took approximately 2 weeks total. Several parts did not come in as soon as expected, causing delays in some of the construction that took place during this period. Issues were also encountered while attempting to set up QGroundControl on the Pixhawk.

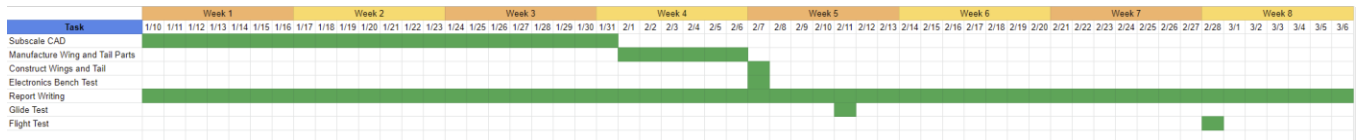


Figure 3: Gantt Chart for C Term

D Term (3/14/2022 – 5/4/2022) unfortunately did not go entirely as planned. QGroundControl proved to be an unfeasible option for an autopilot software, so Mission Planner was selected in its place. The transition between the two software took additional time. CAD took longer than expected, which resulted in a delay in construction. Initially after construction began, the aircraft was damaged in a fall, resulting in delay in further construction.

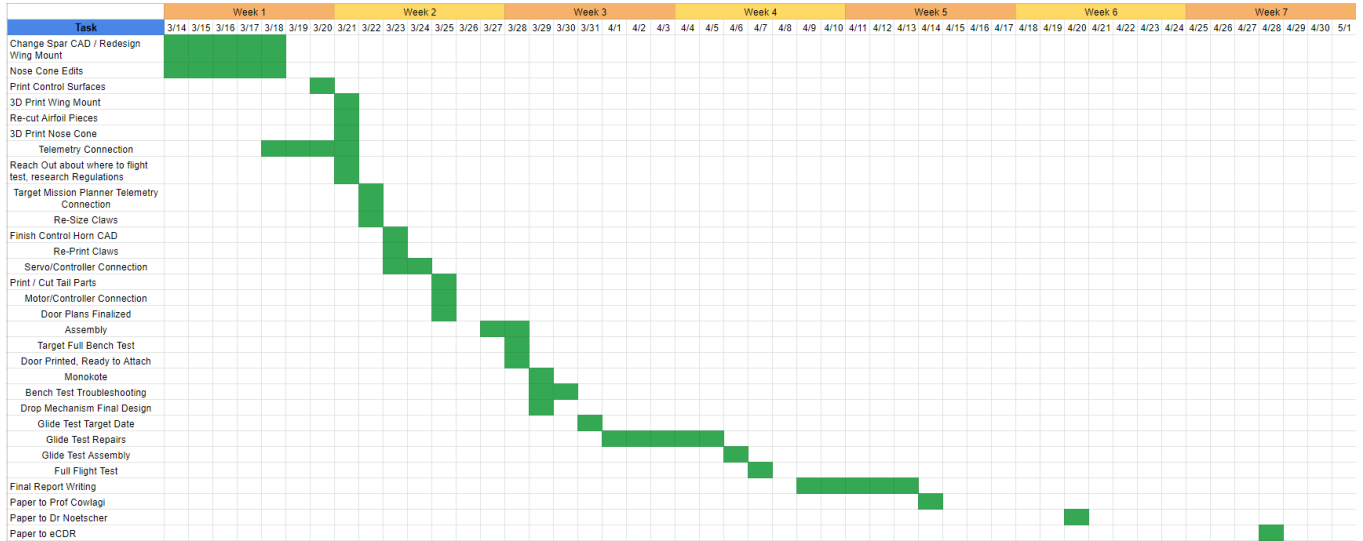


Figure 4: Gantt Chart for D Term

1.5 Relevant Engineering Standards

Many common engineering standards were utilized throughout our project. The NACA standard airfoils database was used for the wing and tail for the aircraft, and ANSI C18.3M for portable lithium batteries were used as well. A third standard used was NEMA ICS 16-2001 for standard servo motors. The NACA airfoil base was mainly utilized in design and analysis, and ANSI and NEMA ICS were used while working on the subscale model build.

1.6 Methods

Listed in Table 1 are the methods used in completion of this project, as well as a brief description of how they were employed.

Table 1: Methods Used for Project Completion

Method	Applications
Ecalc	This program was used to determine electronic flight characteristics such as current drawn, battery life, and maximum voltage.

Mission Planner	This program was used on the Pixhawk to gather flight data and calibrate the aircraft control surfaces.
SolidWorks	This software was used to design the subscale model in its entirety using CAD. It was also used to simulate rudimentary mass properties and determine/adjust the position of the center of mass.
3D Printing	3D printing was used to manufacture various components of the airframe, including but not limited to the control surfaces, wing mount, nosecone, and payload deployment mechanism.
Laser Cutting	Laser cutting was used to manufacture the ribs for the wings, empennage, and control surfaces of the aircraft.

1.7 Broader Impacts

1.7.1 Health, Safety, Welfare

A large impact of the autonomous delivery system is the potential for saving human lives. “According to the Under Secretary of Defense for Research and Engineering, Dr. Michael D. Griffin, “52 percent of battlefield casualties occur when sustainers are delivering needed supplies to and from the battlefield.” [9]. Use of AVs in the Army National Guard could be implemented in response to emergencies and natural disasters. Not only could autonomous vehicles increase reaction time, but they could also allow for safer alternatives than sending manned aircraft or ground vehicles into a potentially unsafe area [10]. Currently, autonomous delivery is used more often in structured environments. A current area of research and development is utilizing autonomous delivery in unstructured environments. This research has led to developments in driverless vehicles made for making deliveries to remote or contested areas [11]. If implemented more regularly in the military, these autonomous vehicles could be sent into hostile areas without compromising any people. The threat of a vehicle, land or ground, being shot at is imminent, and with this technology the officers away from the front lines would be able to set coordinates for the

drop and have an aircraft make the delivery without a pilot. Another aspect of health and safety that autonomous delivery provides is assistance in the field. Some uses are casualty evacuation, delivery of critical supplies, and even applying tele-health to the troops on the ground. (Ivanova, Ksenia, et al.).

1.7.2 Social and Economic Issues

UAV parcel delivery has been a prominent topic of technological discussion since 2013 when Jeff Bezos announced that *Amazon* was going to utilize unmanned vehicles to start delivering packages. There are two main restrictions when it comes to using multirotor vehicles for deliveries [11]. Unmanned delivery vehicles alone may not be a feasible solution for all home deliveries, but as Li et. al. discuss, a combination of a vehicle and UAV working in tandem showed the potential to save costs for the delivery company and also limit the CO₂ emission from delivery vehicles by helping to facilitate the delivery process. A "parallel processing" strategy was employed so the UAV had a home base at the delivery vehicle, and the UAV went on its own delivery while the truck had its own route.

1.7.3 Economic Impacts

Utilizing Autonomous vehicles in industry can increase predictability in the supply chain. Tracking systems and sensors could be implemented to improve assess visibility, and all the data collected is used to make more informed decisions in logistical planning (Ivanova, Ksenia, et al.). Using a larger scale autonomous delivery vehicle could allow retail stores to receive their products from the distributor faster and there could be a shorter turnaround time for getting the next shipment out as well. Using an unpiloted aerial vehicle will create a more predictive environment for supply chain logistics [12]. With a predictable schedule management can put their employees in the best position to succeed and have the most efficient work schedule as possible. The aircraft delivery system would be more precise in the time it takes to get from one point to another than using a less predictable method like a tractor trailer truck. The factors that come into play when driving long distances would far outweigh the factors that would affect the time of flight.

1.7.4 Potential Areas of risk and concern for Autonomous Delivery

While there are many benefits to transitioning both civilian and military delivery systems, potential issues in flight could compromise the effectiveness of the delivery style. For example, if a part breaks mid-flight the autopilot may not be able to recover, where as a pilot on a manned vehicle may be able to use knowledge and experience to safely finish or abandon the mission. Another area of potential concern is the accuracy of sensor data and sensor failure. Most sensors like GPS modules, accelerometers, and rate gyros are small and fragile pieces of equipment. If one or more of the sensors that the autopilot or remote controller need to make a decision with breaks, there may not be enough information for the aircraft to continue effectively flying on the mission. A third potential area of concern is changes in the mission after takeoff. This mainly affects pre-determined, fully autopilot missions. If an aircraft has preset waypoints and an obstacle moves into the flight path of the aircraft, it will not be able to use any collision avoidance mechanisms as passive autopilot generally does not use closed loop feedback.

Along with in-flight problems, general maintenance will also need to be considered when deploying large fleets of autonomous delivery vehicles. These vehicles will be slightly different, mainly in the electrical aspects of the design, and the Army or another company would need highly skilled and knowledgeable crew members to maintain and repair the autonomous vehicles. This would not be a long-term issue, but it is something to consider when planning for deployment [9].

2 System Design

2.1 Final Physical Design

The final prototype was constructed on a 1:10 scale to the actual airframe and weighed a total of 1.9 kg. This scale was picked for ease of conversion of measurements from the full-scale model, as a 1:10 scale would simply require moving a decimal. A 1:10 scale would also be feasible to produce in the facilities available at WPI. This scaling made the design process go much smoother than it would have had a different scale factor been selected. Due to time constraints, defective components, and the fact that only a glide test would be feasibly achieved by the end of the term (as opposed to controlled and/or powered flight), the servos and control wires were omitted from the final prototype. Figure 5 shows the final build of the aircraft that was used in the glide test.



Figure 5: Completed Sub-Scale Build

The fuselage was made from quarter-inch thick balsa wood ribs affixed to a carbon fiber spine running down the length of the aircraft. The ribs were further held in place by carbon fiber stringers through the circumference of each rib. The ribs were created via laser cutting. The fuselage is shown in Figure 6.



Figure 6: Final Fuselage Design

Similar to the fuselage, the wings were made by first laser-cutting ribs out of quarter-inch balsa wood. Three types of rib were produced for the wing: one full-length airfoil cross-section, another with the trailing edge clipped off to accommodate the control surfaces, and a third full-length cross section with a rectangular hole to accommodate a servo.

Carbon fiber dowels were used as spars to help prevent the wing from flexing too far in flight and snapping under the load of the aircraft. Carbon fiber was selected because of its high strength and low weight. These carbon fiber dowels and ribs were affixed to each other by using hot glue. The glue was applied generously around each of the holes in the rib to make sure the balsa wood piece was well secured to the carbon fiber dowel. The frame of the wings (the ribs and spars) was enclosed in a Monokote skin. The ailerons (control surfaces) were 3D printed out of PLA plastic

with the control horns directly incorporated into the design of the parts (as opposed to being a separate part). This was done to ensure a stronger connection between the control horn and the control surface, as there was risk of the two becoming separated during flight if they were to have been separate parts. The control surfaces were 3D printed because additive manufacturing was the easiest way to produce a part with such a unique shape at the scale of the prototype aircraft. PLA filament was used as it was what was available in the lab.

The ailerons were intended to be mounted on the spar closest to the trailing edge of the wing such that they were able to pivot around it, however the control surfaces did not print properly. As a result, the spar was not able to be inserted. To accommodate the control surfaces, the spar closest to the trailing edge was omitted in final construction and the ailerons were instead taped in place. The shortened “control surface” ribs were mounted along the lateral axis of the wing, sandwiched between the servo-mounting rib and a full-length rib on the wingtip. The “control surface” ribs were made so that a small gap was left between the aileron and the wing, allowing for full deflection of the aileron. A close-up image of the left wing is depicted in Figure 7.



Figure 7: Close-up of Left Wing

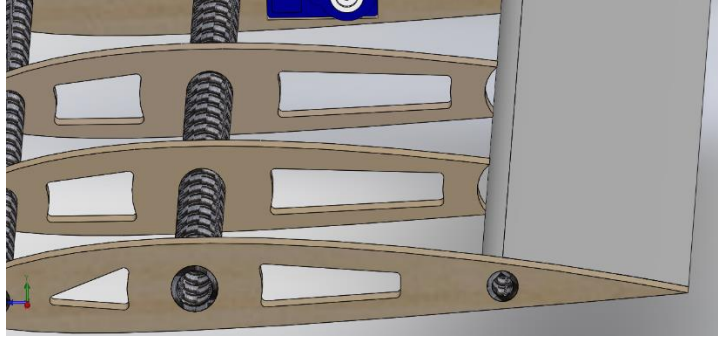


Figure 8: Up-close View of Gap between “Control Surface” Ribs and Aileron (CAD)

The wing was mounted to the fuselage via a 3D-printed mount that was glued to the rectangular spine. The part was designed to slide over the spine and be glued in place, but due to 3D printing issues the bottom section had to be removed and the part was glued to the spine and reinforced with duct tape. The mount had the same cross-sectional shape as the airfoil, which was slightly extruded to provide a mounting surface for the Monokote that would not dramatically alter the shape of the wing at its root. Due to the placement of the duct tape used to reinforce the mount, however, this extrusion was not used. A top and bottom view of the wing mount is shown below in Figure 9 and Figure 10 respectively.



Figure 9: Top View of Wing Mount



Figure 10: Bottom View of Wing Mount

The empennage was constructed in a similar manner to the wings, with laser cut ribs, carbon fiber spars, Monokote skin, and 3D printed control surfaces (in this case the elevator and rudder) and mount. The tail mount was also not properly printed, so servos could not be inserted. Similar to the wings, the control surfaces were taped in place. The control horns of the elevators and rudder did not print properly, so they were removed to reduce drag and to make taping them in place easier. A picture of the empennage is included in Figure 11.

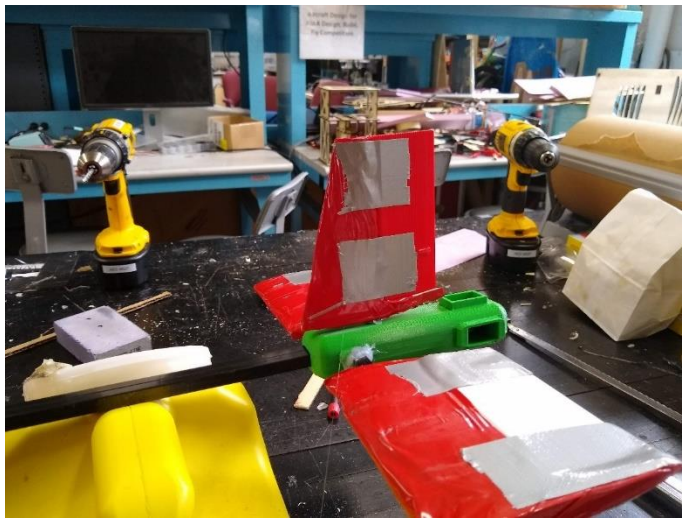


Figure 11: Empennage Assembly

Electronics were placed in the fuselage to get an accurate prediction of the weight distribution within the aircraft. This included the battery, and flight controller, as these were the most significant weight contributors to the aircraft. The motor was not included as it was

unavailable due to extenuating circumstances. The exact placements of these electronics were determined using a weight analysis using SolidWorks described in section 3.1.2.

2.2 Final Electronics

The Pixhawk 4 was chosen as our autopilot flight controller. This controller has many advantages. The Pixhawk 4 is a comprehensive controller that has the necessary sensors built in and has enough connections to servo motors for moving the aircraft's control surfaces. Another reason for choosing Pixhawk 4 is the popularity and amount of documentation. The Pixhawk is a very common flight controller on model airplanes, and there are many websites, video tutorials, and documents that can assist in the use of this device.

The Pixhawk 4 comes equipped with the ICM-20689 and BMI055 accelerometer and rate gyros, an IST8310 magnetometer, and a MS5611 barometer. The servos we decided on using for the prototype's control surfaces are the ACEIRMC SG90 Servo Motor Micro Servos. They are commonplace in model aircraft design while also being cost-effective. The software that the Pixhawk is compatible with are also generally user-friendly.

The initial ground software that was used was QGroundControl. The team ran into many issues with this software. After attempting to fix the errors in QGroundControl, the team made the decision to change mission planning software. The decision to use Ardupilot Mission Planner was made for various reasons. Many other projects have used this platform, reassuring us that people have worked through bugs with the software before. Ardupilot is an older platform than QGroundControl, so there is deep documentation on their website and online forums to help in the setup and debugging process.

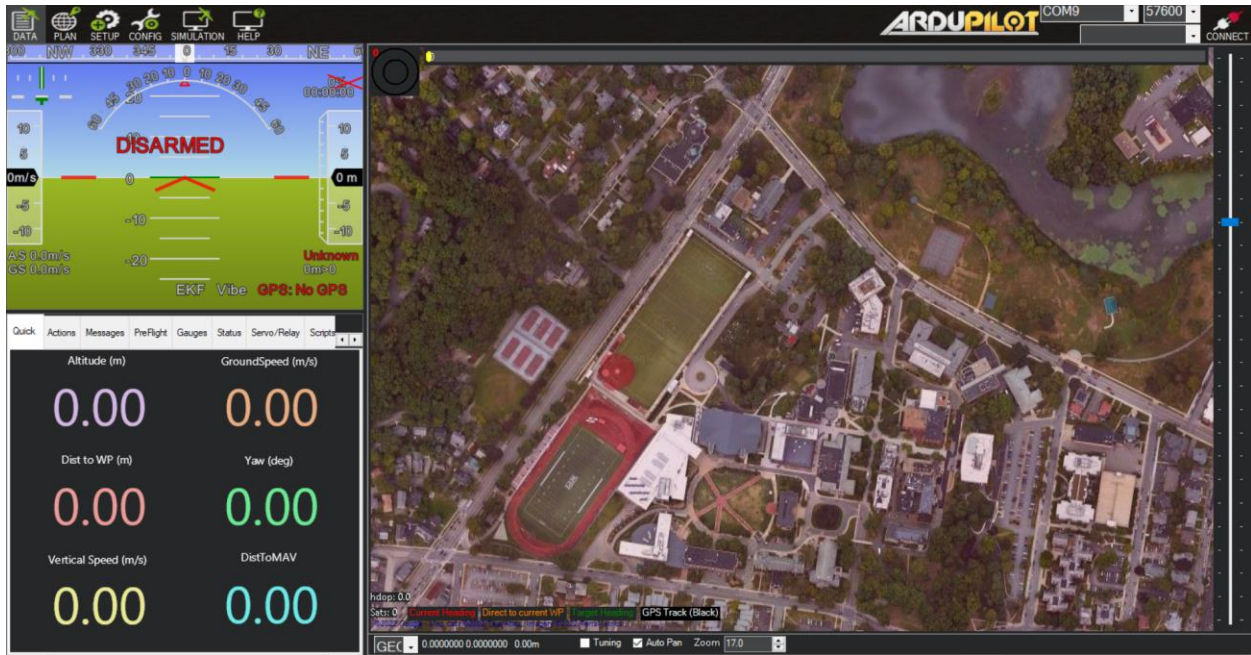


Figure 12: Home Screen of Ardupilot Mission Planner

Setting up the aircraft in Mission Planner is also simple. It involves downloading the specific firmware that corresponds to the vehicle being controlled, and calibrating sensors and the motor. In this case the fixed wing aircraft firmware was installed, and calibrations took place in the lab to ensure that the aircraft was ready to fly. Due to time constraints a full flight test using Mission Planner as the ground software was not able to happen, but a glide test of the aircraft did occur, and the flight data was captured by Mission Planner.

Flight data is automatically recorded and saved in Mission Planner from when the aircraft is armed until it is disarmed. The data files that Mission Planner defaults to are .LOG files. It is possible to review the flight data in graphs in the Mission Planner window, but the team decided to transfer the flight data into .mat files to consolidate the data and be able to plot only the most relevant data in an organized way.

Along with flight data, Mission Planner also offers live in-flight telemetry data. On the left side of Figure 12 is the HUD that shows the aircraft's orientation as well as states such as altitude, airspeed, and pitch angle. This HUD is highly customizable and can easily display the data relevant to the mission.

Planning an autonomous mission in Mission Planner is also a simple process. Below is a sample mission planned to fly around Worcester Polytechnic Institute.

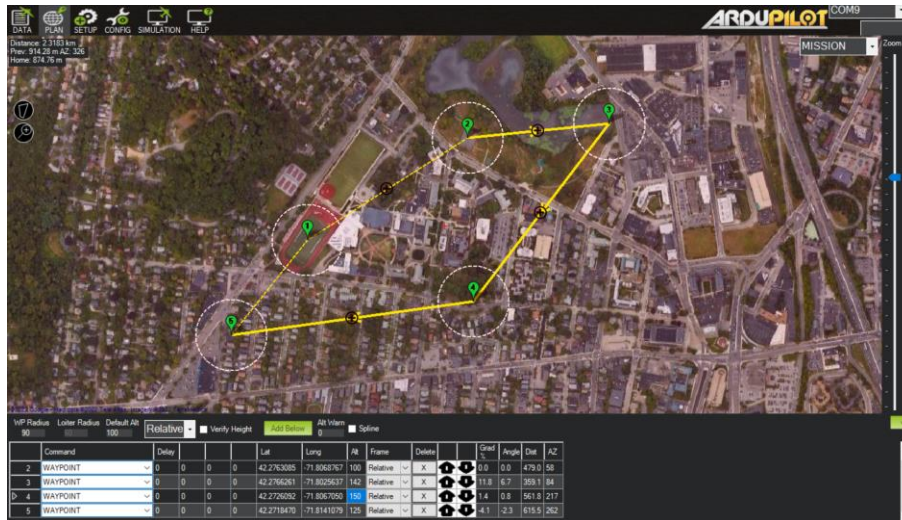


Figure 13: Sample Planned Mission in Mission Planner

The waypoints are adjustable by both coordinates and altitude. There is supplemental information about the flight path to the right of the coordinate information as well. Mission Planner makes it extremely simple to set up an autonomous mission and review what it will look like before flying the aircraft.

2.3 Conceptual Deployment Method

The deployment method will have the aircraft start at a high-altitude cruise until it reaches the target area, then it will reduce engine speed and start a shallow diving glide towards the objective area. Once over the objective area at the proper altitude it will open its bomber doors and release the desired payload. The payload will utilize a static line parachute to reduce complications of the deployment.

Based on ATP 4-48 from the Department of the Army, our deployment system will use the current standards for a door bundle. A door bundle is what the Army calls a payload or package that is deployed out a door, either out the back of a KC-130 or out the door of a helicopter. These deployments rely on gravity to deploy the parachute. For deployment out the back of a C-130, the parachute deployment chord is hooked onto the static line in the aircraft. The aircraft's nose will then be tilted up so that the package starts to slide out of the back of the aircraft. As the package exits the back of the aircraft, the weight of the package deploys the parachute. There is no mechanical components or controls to deploy the parachute, it only utilizes gravity. This lack of

mechanical parts to deploy the parachute significantly reduces the chance of a misfire with the parachute not opening, it just relies on how well the parachute was packed.

The most logical deployment method for our project would be a high-velocity airdrop. The package drops at a rate of 70-90 ft/s. This speed mitigates drift, while staying accurate and allows for petroleum fuels and ammunition to be deployed from the air with a structure around the container. The structure around the dropped container usually has a few different options. One is a honeycomb style structure that compresses as the package hits the ground in order to disperse the force of impact on the box. The other option is to have felt or cellulose wadding inside the package. The force dispersal material depends on the load requirements and the types of parachutes used to slow the speed of the package.

3 Design Process and Analysis

3.1 SolidWorks Modeling

The previous MQP created three aircraft designs to complete a similar task outlined in the project objectives. The three aircraft included a para-wing, fixed wing, and hang glider. The previous team recommended continuing work on their para-wing and fixed wing designs to create a working model of the aircraft and mission objectives.

The mission objectives changed slightly for the continuation of the project. The previous designs were created in mind of only one payload, and our objective was to be able to drop multiple payloads. The total weight of the payload remained the same between the projects, so only slight modification would be needed to fit the geometry of the payloads.

Of the previous designs of the past MQP, our team decided to focus on modifying the fixed wing design. The previous year's fixed wing design can be seen in Figure 14.

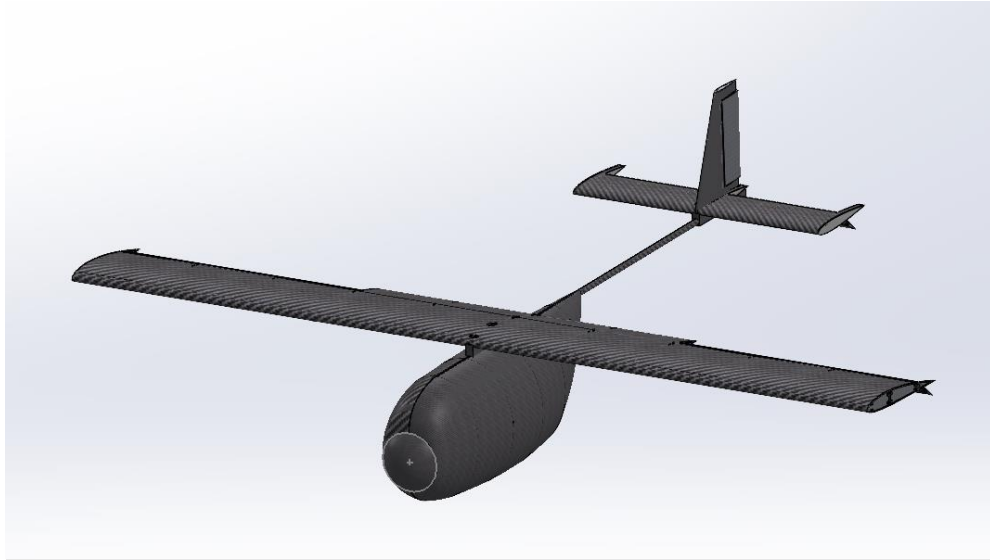


Figure 14: Previous Fixed Wing Design

The new design borrows substantial information from the previous aerodynamic analysis of the previous fixed wing, as the aircraft are similar. As with the previous design, it shares similar payload capacities and ranges as the Cessna 182. It is designed to work with a single propeller engine. The CAD model includes a nose cone in place of the engine and propeller to make the modeling process simpler. The CAD for the full-scale aircraft can be seen in Figure 15.

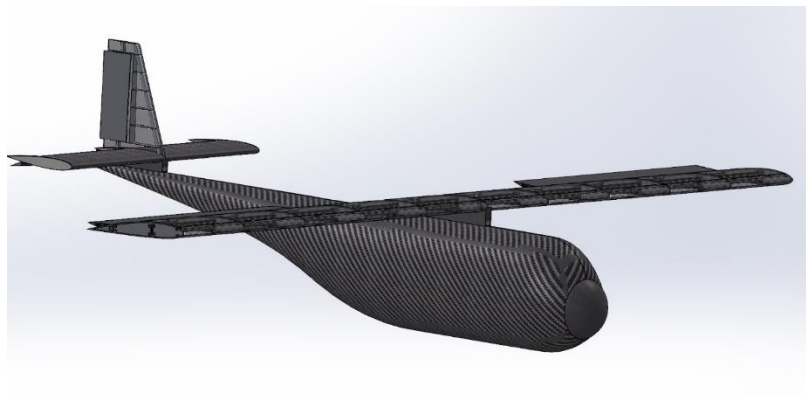


Figure 15: New Fixed Wing Design

Much of the geometry and design characteristics remain the same between the old and new designs, as the wing and tail remain largely unchanged. The wing and tail geometry were designed

to work within the mission requirements, so the main changes were to the fuselage to account for the size of the payloads.

One of the main focuses for this project was to create a sub-scale model of the aircraft, so a detailed rendering of the sub-scale aircraft was created using Solidworks to aid with the construction. The model can be seen in Figure 16. While creating the model, planning the construction was a necessary step while converting the full-scale to the sub-scale. Section 3.1.3 describes the decisions made for each part of the sub-scale model.

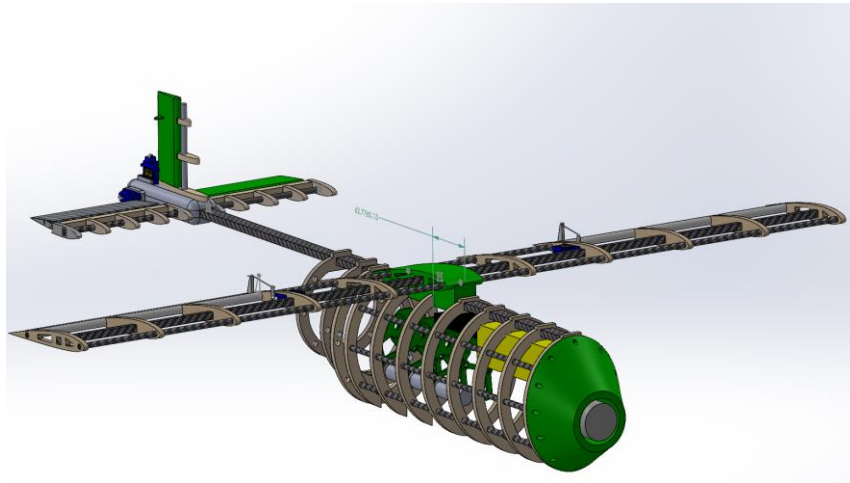


Figure 16: Detailed Model of Sub-Scale

Using the detailed model, the horizontal stability and total weight of the sub-scale could be found. This is outlined in section 3.1.2, where the SolidWorks models were created to find out the optimal locations for electronics and weight placements.

3.1.1 Design Process of Fixed-Wing

The new design involved changes to the fuselage to allow for more spread-out weight. The total weight of the aircraft was not changed, as it would require new analysis and changes to the wing and tail. The most important aspect to calculate when changing the weight distribution is how the neutral point would change. Section 3.1.2 shows the calculations used to find the neutral point and ensure the aircraft will remain stable. To make sure the aircraft remained the same weight, an iterative process was used when designing the new fuselage, to get the desired weight and center of mass.

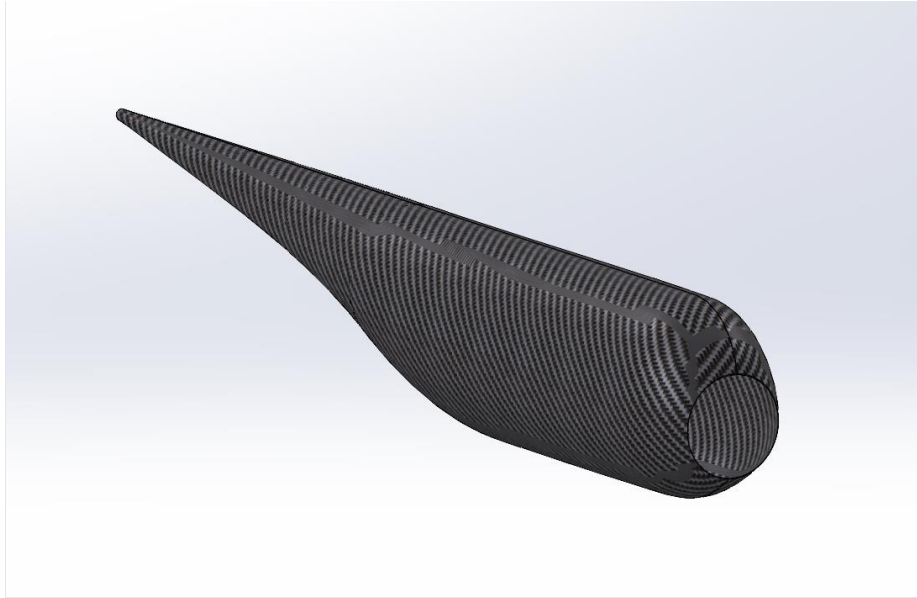


Figure 17: The Redesigned Fuselage

To create the new fuselage, the general shape was taken from the old design. The cargo area in the old design was extended in the new design to flow extending through the entire aircraft, tapering off to the tail with a tangent curve. Because of the change of distribution of weight, the fuselage needed to be extended to maintain the same location for the center of mass. The total length of the fuselage is 8.58 m. to account for the increase in weight, the maximum height of the fuselage was reduced from 1.46 m to 1 m.

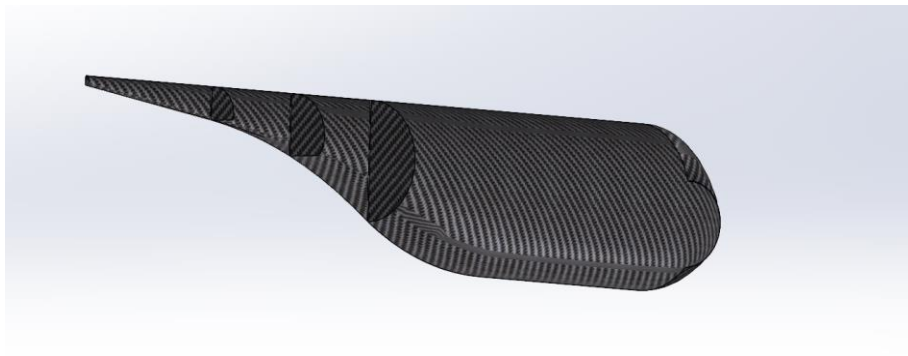


Figure 18: Shell of Fuselage

To maintain a similar mass estimation between the two fuselages, the structure was shelled to have a wall thickness of 2mm, which is consistent between the old and new designs. The actual

wall thickness is likely going to be much greater than that, but that was considered in the mass calculations.

```

Mass properties of FuselageSolid
Configuration: Left Side
Coordinate system: -- default --

Density = 1880.00 kilograms per cubic meter

Mass = 104.78 kilograms
    
```

Figure 19: Mass Properties Estimation of Fuselage

3.1.2 Weight Analysis of Design

To estimate the total weight of the aircraft, the individual components were added together to estimate the total weight of the aircraft. To account for the extra weight added from manufacturing and unforeseeable circumstances, the fuselage weight was doubled, as to calculate within tolerances.

Table 2: Mass estimations of full scale

	Individual Mass (kg)	Quantity	Total (kg)
Wing	184.47	1	184.47
Vertical Tail	47.26	1	47.26
Horizontal Tail	73.32	2	146.64
Fuselage	200	1	200
Engine	100	1	100

Payload	250	1	250
Total Dry Mass			705.45
Fuel	270.70	1	294.55
Total Takeoff Mass			1000

The total takeoff mass was estimated to be 1000 kg. This was the same as the previous design, so it was known that the wings would generate enough lift for the mission. This estimation was very helpful when scaling the aircraft, as we knew what a 1:10 scale aircraft would approximately weigh.

To estimate the mass of the sub-scale design, the mass estimation needed to be scaled down by 10^3 . Table 3 shows the estimation of mass of the empty aircraft.

Table 3: Mass estimations of the Subscale model

	Individual Mass (kg)	Quantity	Total (kg)
Wing	.18447	1	.18447
Vertical Tail	.04726	1	.04726
Horizontal Tail	.7332	2	.14664
Fuselage	.200	1	.200

Payload	.25	1	.25
Total Dry Mass			.82837

The total empty mass of the model is estimated to be 828 g, which is within the desired weight of around 1 kg. This was a rough estimation, and a detailed model was created to understand how the sub-scale would be constructed. The detailed model can be seen in Figure 20.

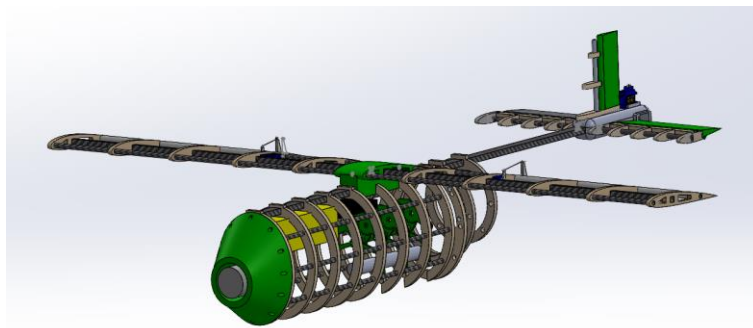


Figure 20: Detailed Model of Sub-Scale

Each part of the detailed model was edited to have the same density of the material the part would be made of. The total weight of the subscale is estimated to be 2.68 Kg. The mass breakdown of the sub scale can be seen in Table 4.

Table 4: The mass breakdown of the sub scale model

Part of Aircraft	Weight (Kg)
Fuselage	0.429
Tail	0.378
Nosecone	0.221
Dropping System including payload	0.275
Motor	0.231
Battery	0.487

Wing	0.595
Pixhawk	0.015
Servos, wiring, misc.	0.050
Total:	2.68

With the accurate weight estimation of the sub scale, the placements of the electronics could be determined. The electronics were placed so that the center of mass is always ahead of the neutral point of the aircraft. The neutral point fraction was calculated as 0.399. This means that for the subscale the center of mass must be less than 60 cm behind the leading edge of the wing. Equations 1 and 2 calculate the neutral point fraction, where $C_{L\alpha}$ and $C_{L\alpha,t}$ are the stability derivatives of the wing and tail, \bar{V}_H is the volume ratio, h_{ac} is the location of the aerodynamic center, and $k_{\epsilon,\alpha}$ is an empirically determined constant.

$$h_{np} := h_{ac} + \frac{C_{L\alpha,t} \bar{V}_H}{C_{L\alpha}} (1 - k_{\epsilon,\alpha}) \quad (1)$$

$$\bar{V}_H = \frac{S_t}{S} \quad (2)$$

The SolidWorks model was used to find the approximate center of mass. The electronics were then placed in the model so that the aircraft would maintain stability after every drop.

The battery was also placed toward the front of the aircraft, as to offset the weight from the tail. The Pixhawk and Payload system are close to the center of mass, as the payload system will be changing mass, and the Pixhawk needs to be as close to the center of mass as possible.

To estimate how the center of mass changes for each payload drop, the masses of all the components of the subscale were added to the detailed SolidWorks model. The center of mass was then calculated by SolidWorks and shown on the assembly. To measure where it changes and to make sure it remained in front of the neutral point, a smart dimension was added from the leading edge of the wing to the center. Table 6 shows how the center of mass changes on each drop.

Table 5: Center of Mass after Payload Drops

Drop State	Distance between LE of wing and Center of Mass (cm)
------------	---

Fully loaded	4.0
First drop	3.99
Second drop	3.98
Final Drop	3.99

Because the payloads are close the center of mass, they have a minimal effect when they are dropped from the aircraft. As calculated previously in this section, the neutral point was shown to be 6 cm behind the leading edge, so the aircraft remains stable.

3.1.3 Individual Parts of Model

This section will go over each major component of the design and explain the reasoning behind the design decisions. All these sections were created at first by scaling the full-scale model to 1/10th the size and edited to work in an assembly.

The fuselage was the first part to model for the sub-scale, and it was created by using the sketch tool to draw ribs on the full-scale model. These ribs were then extruded to be the shape of the full-scale fuselage. The width of the ribs is 0.25 inch, as that is the thickness of the balsa wood that we would cut. The distance between each rib was created to be 50mm, as that was the distance from the nose to the main body.

After all the ribs were created, they were moved to be their own individual parts that could be edited and put together in an assembly. In these individual parts, holes were put in around the diameter of the rings, as carbon fiber supports would hold the ribs together. This initial assembly can be found in Figure 21.

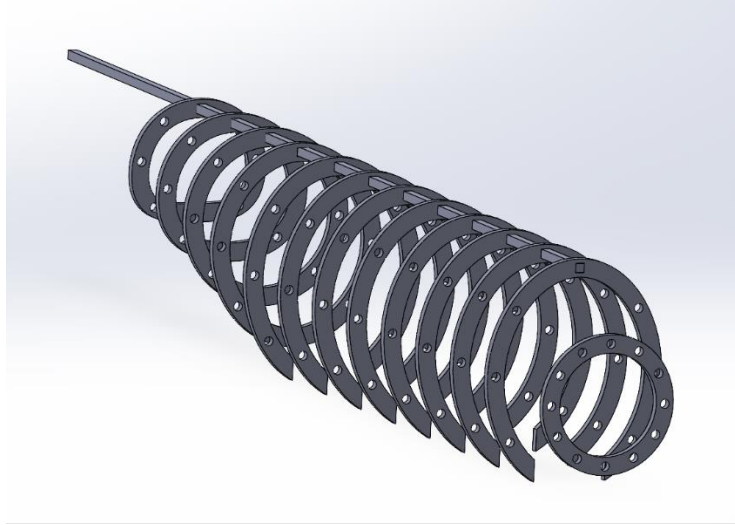


Figure 21: Initial Assembly of Sub-Scale Fuselage

The top support of the assembly was determined to need to be a rectangular rod as to make attaching the wings and tail more secure. This top support was named the “spine” as it would connect everything in the assembly together.

The thickness of the holes is 6mm in diameter, so the overall thickness of each rib is 12 mm. This was changed after making some test parts using scrap on the laser cutter. The need for a nose piece was also apparent, as it was unclear how the motor would attach to the front.

A 3D printed nosecone was determined to be the best solution for attaching the motor to the aircraft. The shape was created by taking the previous ribs and lofting them to be a solid cone. A housing for the motor was created, so there would be a solid body to attach to. Screw holes were made to attach the cone to the main body. The result can be seen in Figure 22.

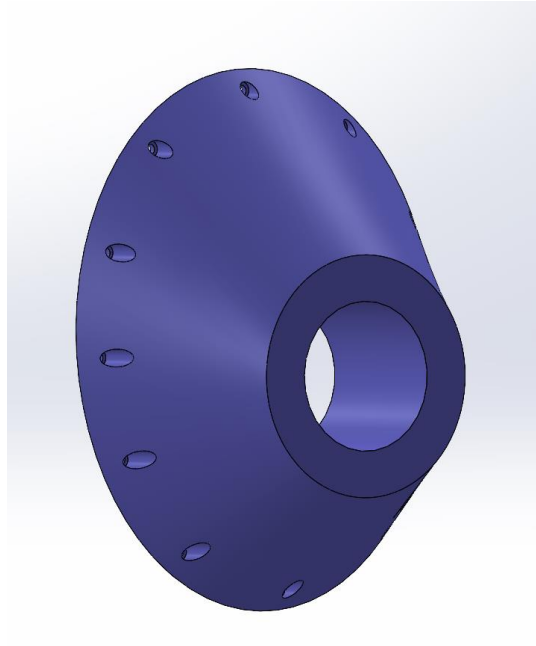


Figure 22: Final Nosecone Model

The final product was printed in the Innovation Studio Prototyping lab and was made of PLA. It can be seen in Figure 23. The final part weighs 0.1 kg, and has accurate sizing compared to the model.



Figure 23: Printed Nosecone

The wing geometry remained unchanged from the previous year's MQP, with the modification of being scaled down by a factor of 10. The prototype wing utilizes a NACA 2412 airfoil with a 1 m wingspan, 0.15 m chord length. A new CAD model for the subscale design was created to aid with the construction process. Figure 24 shows the wing assembly modeled in SolidWorks. Originally, the wing was designed with a circular main spar instead of a square one. This was later changed due to a lack of availability of circular carbon fiber tubing. There was extra square rod available from the spine, so the CAD for the wing ribs was modified accordingly and the parts recut.

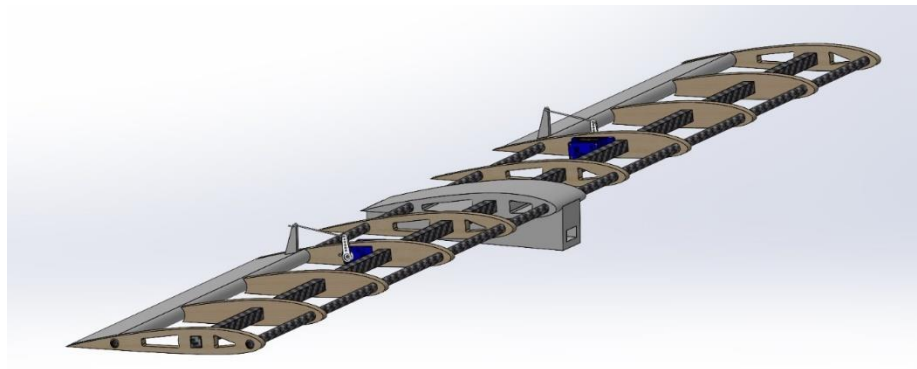


Figure 24: Wing Assembly Model

The wing is separated into 0.25 in balsa wood ribs connected by 3 carbon fiber dowels. The distance between each rib is 105 mm. The three variations of rib used to construct the wing are shown below. The cutouts other than the ones for the spars/servos are a weight saving measure, serving to reduce the overall components' masses without severely compromising their structural integrity.

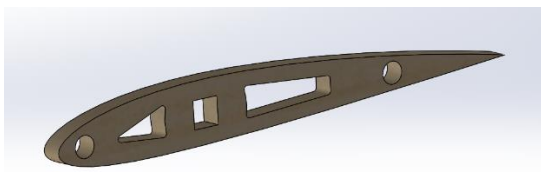


Figure 25: CAD for Full-Length Rib

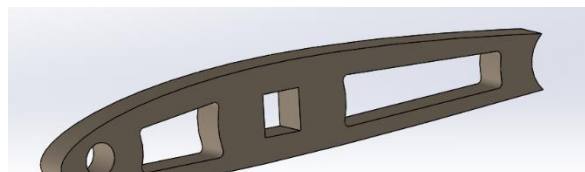


Figure 26: CAD for Control Surface Rib

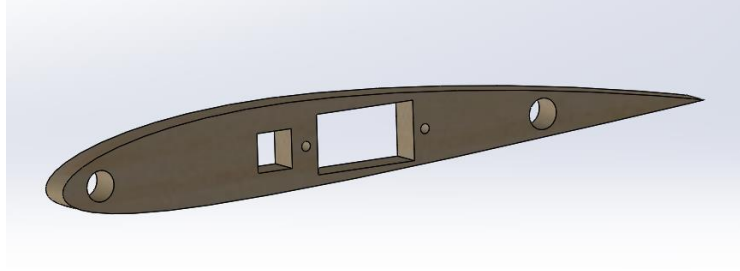


Figure 27: CAD for Control Adjacent Rib

To connect the wing to the spine of the fuselage, a wing mount was modeled. The wing mount can be seen in Figure 28.

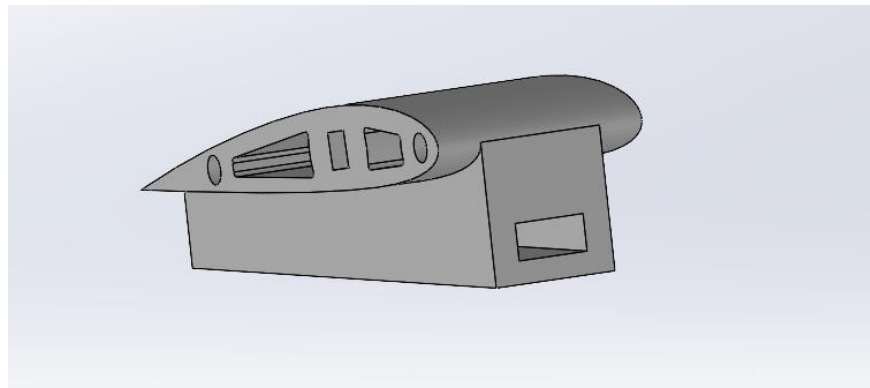


Figure 28: Wing Mount Model

The top part of the wing mount is 48 mm wide as to allow enough support to connect the wing dowels through. The bottom part of the wing mount is 28 mm across, as to give 6mm of support to the main spine connection.

The ailerons are solid pieces of the NACA 2412 airfoil. They are 25% of the chord length, and 300 mm long. Each was given a control horn to connect the servos to. The horn is as tall as the maximum thickness of the airfoil. For this model, they are 20 mm tall. An example of an aileron can be seen in Figure 29.

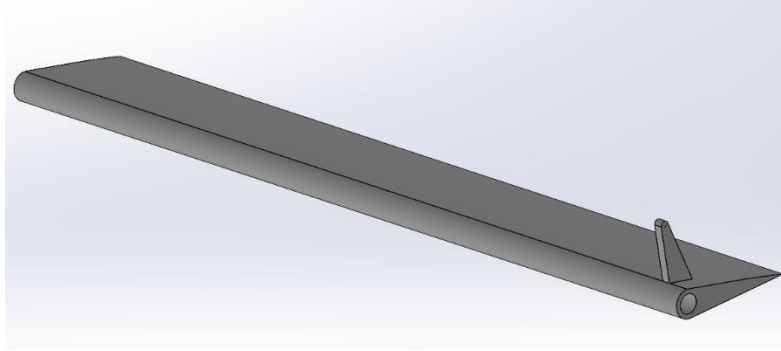


Figure 29: Aileron Model

Similarly, the tail geometry was unchanged from the last year's MQP. The tail uses a NACA 0012 airfoil design. The total horizontal tail span is 340mm, and the vertical tail height is 120 mm. The tail airfoils were divided up into 0.25in balsa wood ribs. Each rib is 38 mm apart. Both the horizontal and vertical tail are supported by a primary carbon fiber dowel and a secondary carbon fiber dowel to support the movement of the elevators and rudders. Figure 30 shows the CAD for the tail assembly.

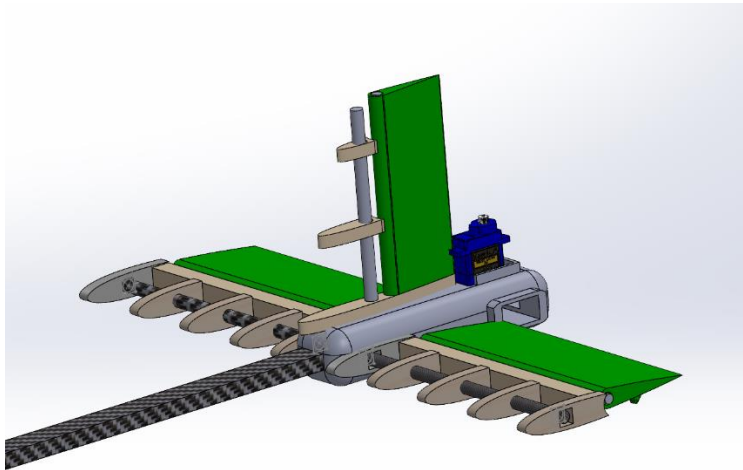


Figure 30: Tail CAD Assembly

To connect the tail to the spine, and to attach the horizontal and vertical parts of the tail together, a tail mount was modeled. The tail mount was also responsible for holding the servos used to control the elevators and rudder. The CAD for the tail mount can be seen in Figure 31.

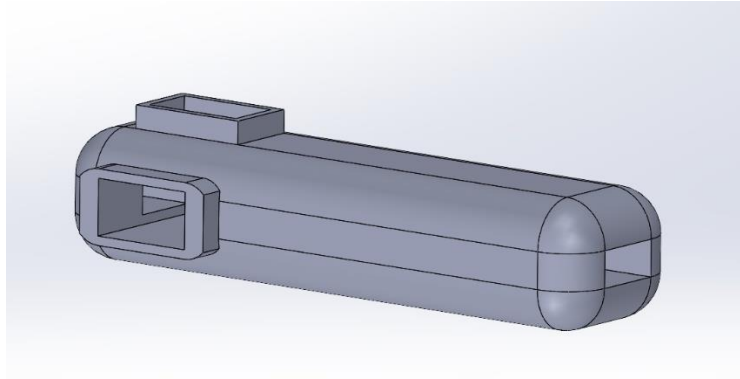


Figure 31: Model of Tail Mount

The total length of the tail mount is 135 mm to account for the chord length of the tail and the servos. The elevator and rudder surfaces were created in a similar manner to the wing's ailerons. The elevators are 140 mm long, and the rudder is 100 mm long.

While a payload retention/deployment mechanism was never fully constructed, a design for one was considered throughout the construction process and is included in this report. Each payload is simulated by a roll of 36 dimes weighing 83 grams each. There are 3 rolls of dimes, totaling a weight of 250 grams. Each roll is contained in a box that is dropped by a servo-actuated claw. The payload container is held in place by the claw which clamps into notches in the sides of the container. The static line of the payload's parachute is affixed to the ceiling of the cargo hold to provide a rigid mount to ensure proper deployment of the chute. The doors to the cargo hold are actuated by a single servo. The doors are connected to the servo arm via rigid wire, similar to the control surfaces on the wing. When the servo arm is rotated up, the doors are shut, whereas when the servo arm is rotated down the doors are fully open, allowing for the payload to be released.

Before attempting construction of the main deployment mechanism, the team constructed a model of the deployment mechanism to test size and functionality. The payload retention bay was constructed out of foam, and the claw was 3-D printed. The mechanism was triggered by programming an Arduino Uno microcontroller to rotate the servo to open the claw, then reverse direction to close it. Figures 32 and 33 below show the test mechanism parts and assembly.

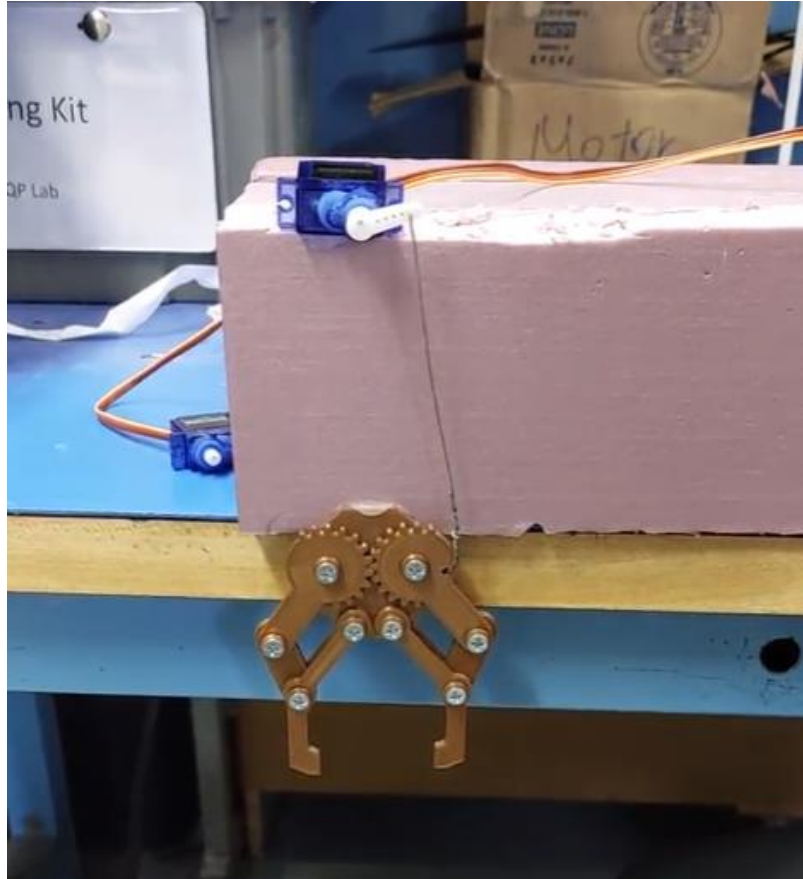


Figure 32: Dropping Mechanism Prototype

The design of the claws is from the author 'GnarlyDesign' uploaded to instructables.com. The design was imported to SolidWorks to be added to the subscale assembly. A rough rendering of the mechanism can be seen in Figure 33.

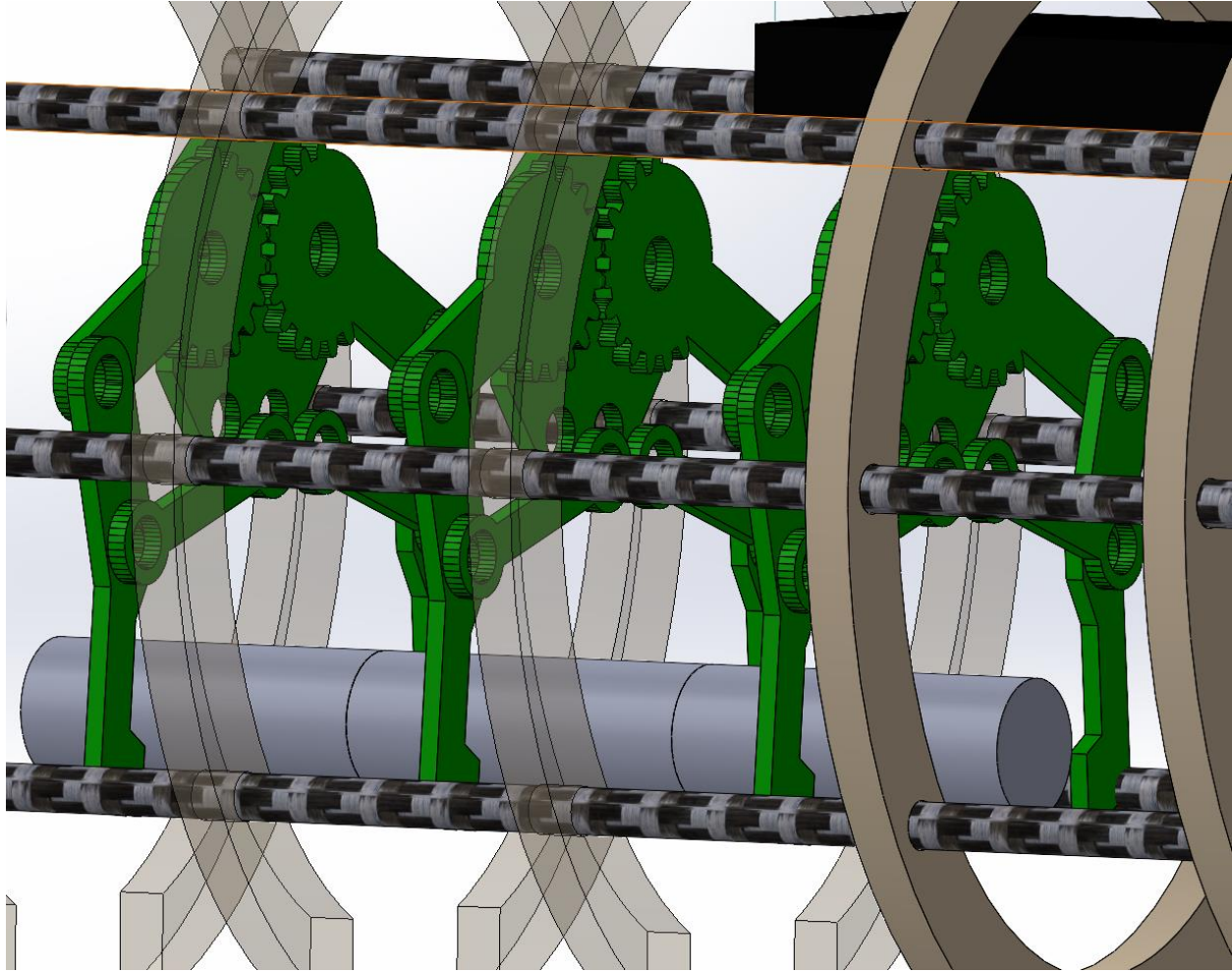


Figure 33: Rough Model of the Dropping Mechanism

The middle portion of the circumference of the fuselage ribs underneath the dropping mechanism was removed to accommodate dropping of the payload. The total estimated weight of the system including the payloads is 300 grams. The placement of the mechanism is as close to the center of mass of the aircraft as possible. This was chosen because as the payloads are dropped, the location of the center of mass would change. If the payloads are in the center, this would minimize the effect.

3.2 Construction Process

There were multiple phases to the construction process, and we went through two different iterations of materials. The first iteration utilized foam insulation board as the main structural component in the aircraft. The idea was that the foam board would be easy to mold into the shape we wanted while being able to cut out slots we needed for the electronics. We started by hot gluing multiple layers of foam board together making a 3-2-3 stack because the foam board itself wasn't long enough to cover the necessary length of the aircraft. The foam board was then placed under a metal sheet with a forty-five-pound weight on top of it to make sure that the hot glue properly adhered to the material. This foam board stack was then shaped into a cylinder using both an insulation knife and a hot wire cutter. Once the foam was made into a cylinder, it was then cut to put in the shape and angle used for the progression from the fuselage to the tail. It was then finished off by using different grit sandpaper to make the fuselage smooth. The pictures documenting our progress on this iteration are below.



Figure 34: 3-2-3 Stack of Foam Board (Uncut)

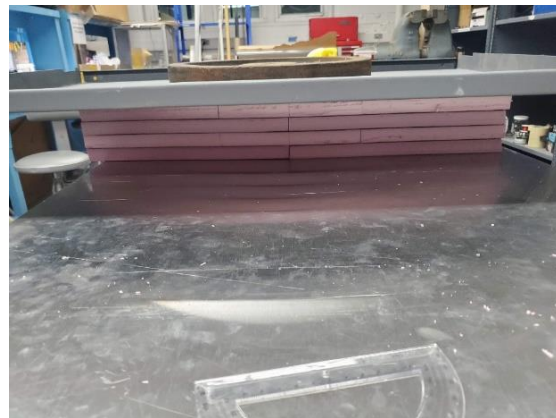


Figure 35: Using a weight and metal plate to ensure the hot glue adhered properly



Figure 36: Foam board cut to the width needed for the fuselage



Figure 37: Side view of cut foam board



Figure 38: Face of the cut foam board, scored to see necessary shape and dimensions of the resulting cylinder

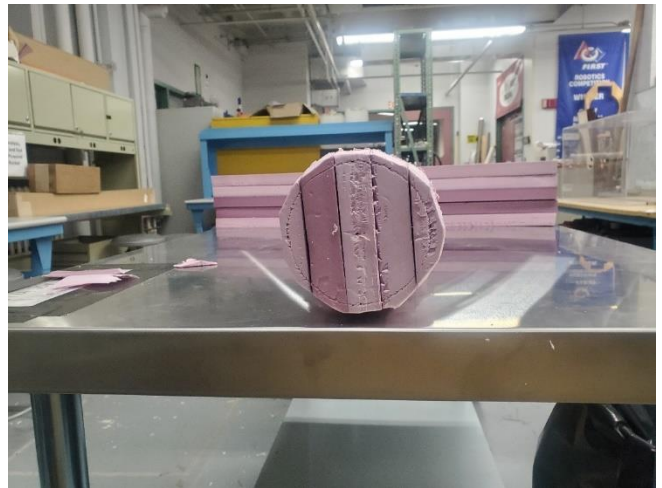


Figure 39: Front view of the foam during cutting process

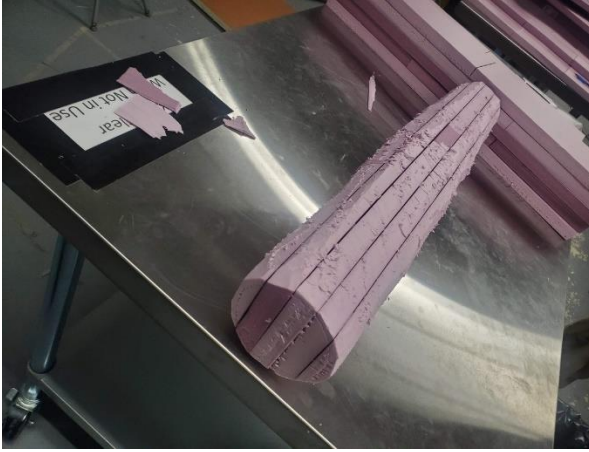


Figure 40: Top-down view of the foam board cut and shaped

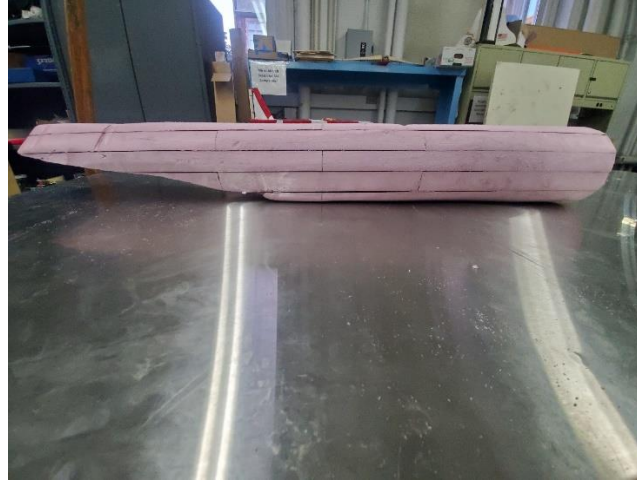


Figure 41: Finished foam board fuselage

We only got to the shaping portion while using the foam board because as a team we decided that it would be better to use carbon fiber and balsa wood as the main elements in construction.

Iteration two utilized carbon fiber rods as the main structural support and balsa wood was used as ribs lining the body. The nosecone, wing mount, tail mount, and control surfaces were all 3D printed. The first part to be manufactured was the ribs for the fuselage wing, and tail, which were cut using a laser cutter. The dimensions for the cut were taken directly from the sub-scale CAD. Figure 42 shows the first batch of parts from the laser cutter, used in the final construction. Figure 43 and Figure 44 shows the vertical and horizontal tail being laser cut along with some spare fuselage ribs.



Figure 42: Laser Cut Fuselage and Wing ribs

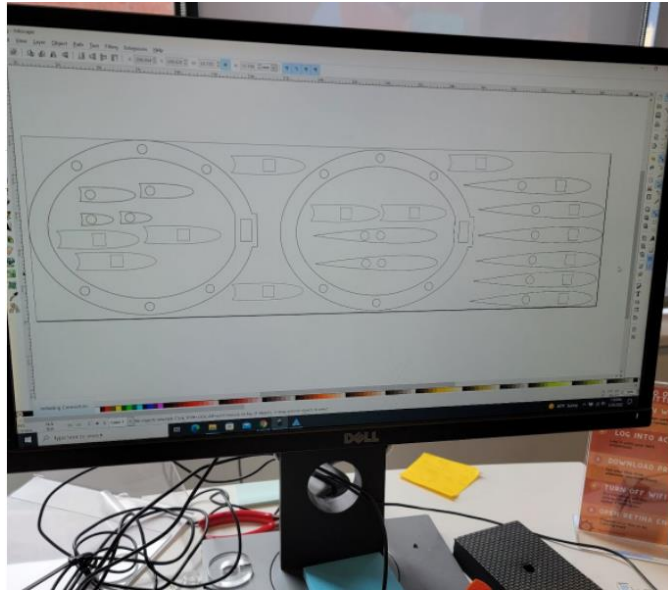


Figure 43: Laser Cutting Tail Pathing

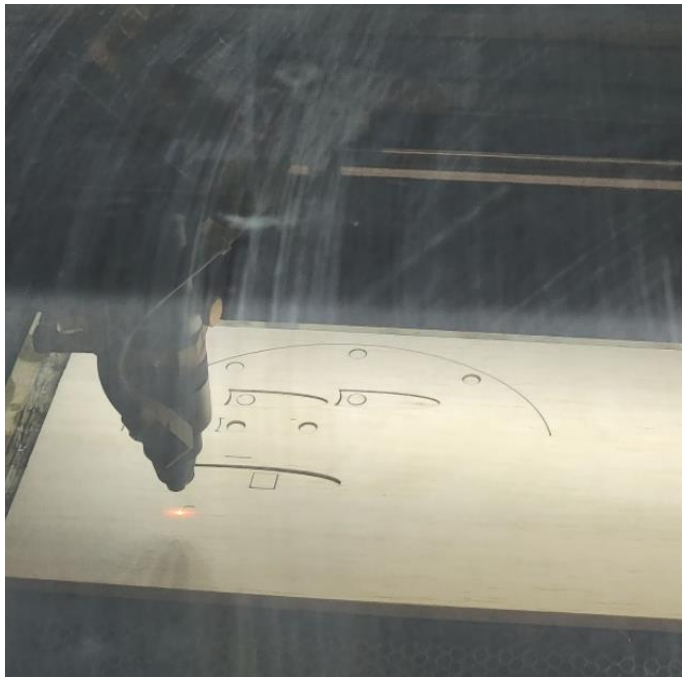


Figure 44: Laser Cutting Tail

Extra parts were manufactured for all aspects of the aircraft, as to give room for error. While the ribs were being cut, the nosecone, wing mount, tail mount, and control surfaces were 3D printed. Each part took much longer to 3D print than to laser cut, so multiple printers were used.

The STL files used to make the prints were created from the SolidWorks model. These parts were not as accurate to the model as there were many errors in the printing process. These errors include: the ailerons were warped after printing, too much filler material in the wing mount, the wing mount warping, and the elevators and rudder shrinking compared to the CAD. These errors were determined to be acceptable for the initial glide test and first prototype of the design. Figure 45-Figure 48 shows the printed parts, and early stages of the construction.



Figure 45: 3D Printed Wing and Tail Mounts.

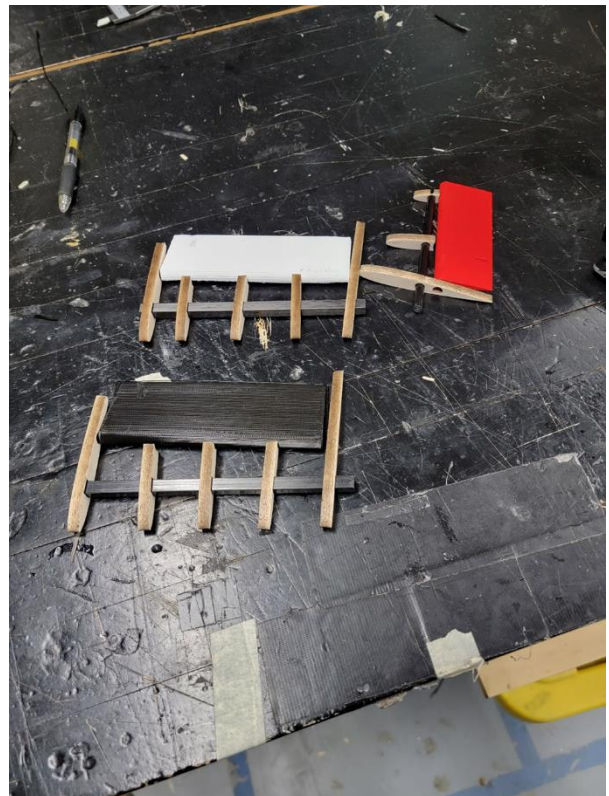


Figure 46: 3D Printed Tail Control Surfaces

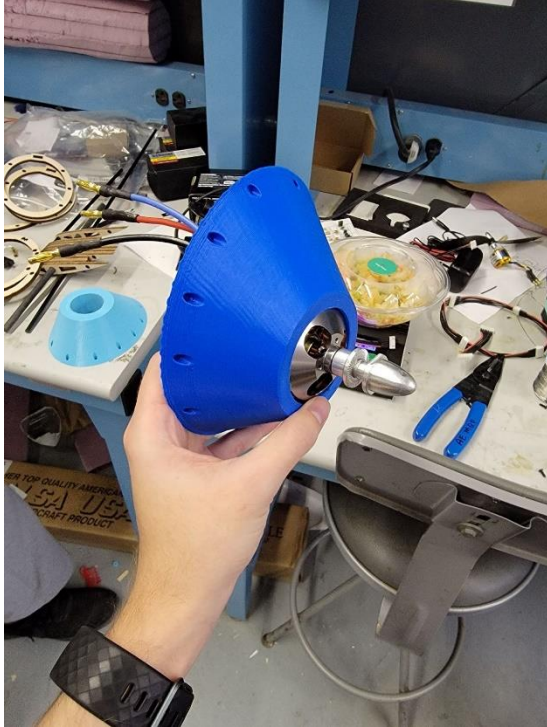


Figure 47: 3D Printed Nose Cone with Motor



Figure 48: 3D Printed Ailerons

The construction started from the nose of the aircraft moving back to the tail of the aircraft. The construction started off by attaching the carbon fiber support rods to the 3D printed nosecone. This was done by placing the nosecone face down on the lab table. The carbon fiber rods were then placed through drilled holes in the nose cone. Once these rods were level on the table, they were then hot glued into place. After the plane was complete the excess carbon fiber that was sticking out the front of the nosecone was cut using a hacksaw and then filed down. Once the carbon fiber rods were secured in the nosecone the ribs were the next to be secured to the frame. To make sure that the ribs were properly spaced, foam board was wire cut to the proper distance, and then placed on top of the necessary rib. Three of these such measuring pieces were cut for use on the ribs. The follow-on rib was then placed on top of the foam measuring pieces to make sure that the ribs were the correct distance. A spirit level was then used to double check on the accuracy and on how even the ribs are. Once the ribs are set up properly, they are then secured with hot glue. This was done for the main section of the fuselage. Halfway up the fuselage, the wing mount was then attached to the carbon fiber spine. Due to a manufacturing error the wing mount was printed improperly so some adjustments to it were made. The bottom half of the wing mount was

cut off so instead of sliding onto the spine, it was placed over it. It was secured by using a copious amount of extra strength hot glue and duct tape. Once the fuselage starts to slim towards the back, the carbon fiber rods were not used due to the elasticity of the carbon fiber rods. These smaller ribs were still secured by the carbon fiber spine. The rest of the smaller ribs were secured by cutting small pieces of foam insulation board to use to secure the ribs at the proper measurements.

The wings were constructed in a similar fashion to the fuselage. The carbon fiber rods were cut to the desired length using a hack saw, finished off with a file and then secured to the wing mount using hot glue. The same rib securing process was used for the wings as the fuselage, using specially cut foam board and the spirit level. To build the tail, the tail mount needed some extra work to be useable. Due to the print shrinking, the middle hole had to be filed for the aircraft spine to fit into the tail mount. Holes were then drilled in the sides of the tail mount to fit the tail pieces and rudder.

With the main body construction completed, a wrapping material was needed to make the assembly more streamlined and aerodynamic. The material we ended up using to cover the aircraft was Monokote. Monokote is a commercially available plastic heat shrink wrap. The process of applying this material to the aircraft started with wrapping the fuselage perpendicular to it. The Monokote started with using an iron on the Monokote on the rib. The iron was used to melt the Monokote to the rib to secure it. Once the Monokote was attached to the ribs, a hot air gun was used to then heat shrink the Monokote to the aircraft to make it a smooth surface that is flush to the aircraft ribs. This process was then repeated on the wings and tail pieces.

To attach the control surfaces to the wings, the sections of Monokote were cut out and the control surface was inserted into the wing. The original plan was to have the control surfaces mounted on a carbon fiber rod that was running the length of the wing. Due to some manufacturing errors, and the team not conducting a full flight test, the control surfaces were duck taped to the wing. The overall construction process and progression is documented in the pictures below.

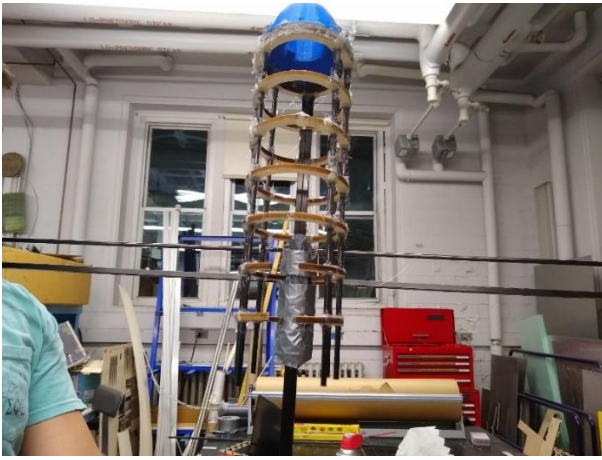


Figure 49: Partially Assembled Fuselage



Figure 50: Process for Adding Ribs



Figure 51: Fuselage with Monokote



Figure 52: Final Aircraft

3.3 Electronics Process

The initial mission planning software the team elected to use was QGroundControl. The many customizable features of QGroundControl allows for the Pixhawk 4 to be effective for many types of mission profiles. QGroundControl makes it easy to plan a mission, connect servo motors to a control surface, and calibrate the onboard sensors. All screenshots of QGroundControl are taken after the aircraft frame was set to be a fixed wing aircraft. Some features may change if the platform is used with a quadrotor or other aerial vehicle.

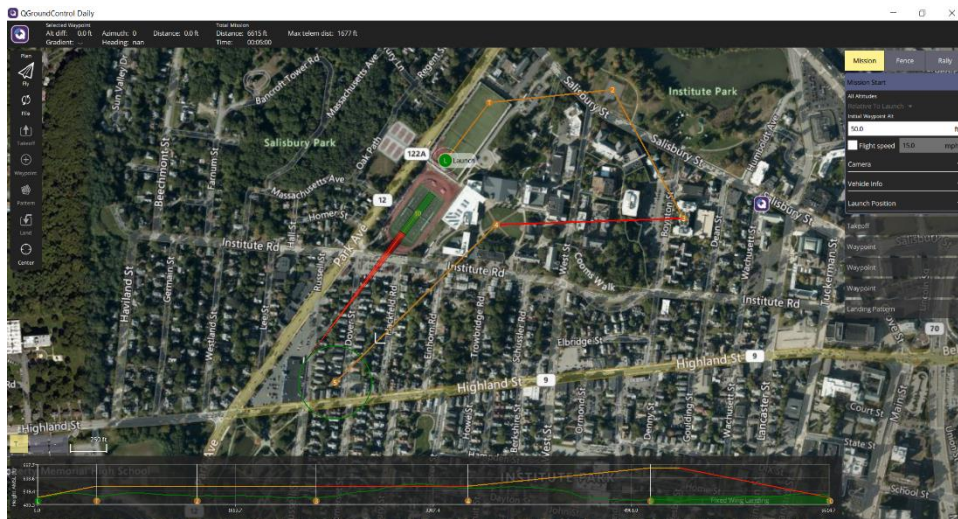


Figure 53: View of a Designed Mission on QGroundControl

Autonomous missions with QGroundControl are highly customizable. Users can set the takeoff distance, speed, and pitch angle. Waypoints are set with the click of a button, and the user sets the height and speed for the aircraft to reach the waypoint coordinates at. There are changes to on board cameras that are also available when the aircraft reaches a waypoint

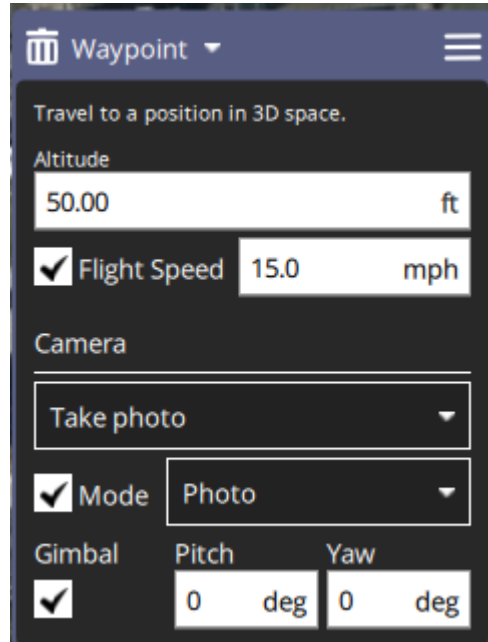


Figure 54: Waypoint Customization in QGroundControl

The landing pattern is also a highly customizable feature. The user can set parameters such as the loiter altitude and radius, as well as the landing maneuver distance and glide slope.

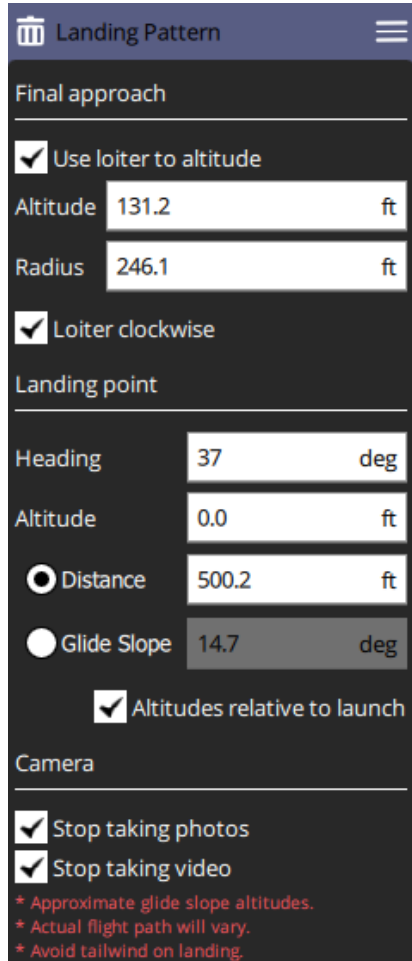
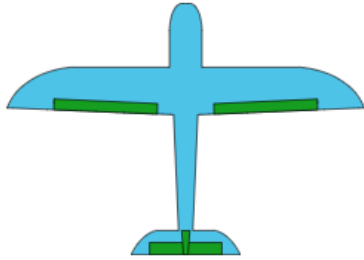


Figure 55: Landing Pattern Customization in QGroundControl

The team utilized micro-servo motors to control the control surfaces and dropping mechanism of the aircraft. Each aileron has its own servo, likewise with the elevator. The rudder was controlled by a singular servo. The bomb bay doors also included a servo to open and close the doors. The servo motors were initially connected to an Arduino Uno for proof of concept, but for the flight test the servos were controlled by the Pixhawk.

The main materials needed to make these connections are a Pixhawk 4, a Servo motor, aircraft, and QGroundControl application. On the Power Management Board (PMB), connect Servo wires to FMU/PWM OUT ports. To determine which ports are available to use, refer to the airframe reference documentation on the Pixhawk 4 website. The group used the “Standard Plane” airframe, and the “Standard Plane” setup. Below is a diagram of the setup and port assignments for the airframe the group chose.

Standard Plane



Common Outputs

- **MAIN1:** aileron
- **MAIN4:** rudder
- **AUX1:** feed-through of RC AUX1 channel
- **AUX2:** feed-through of RC AUX2 channel
- **AUX3:** feed-through of RC AUX3 channel

Name	
Standard Plane	<p>Maintainer: Lorenz Meier <lorenz@px4.io></p> <p><code>SYS_AUTOSTART</code> = 2100</p> <p>Specific Outputs:</p> <ul style="list-style-type: none"> • MAIN2: elevator • MAIN3: throttle • MAIN5: flaps • MAIN6: gear

Figure 56: Airframe and Port Assignments for the Model Aircraft

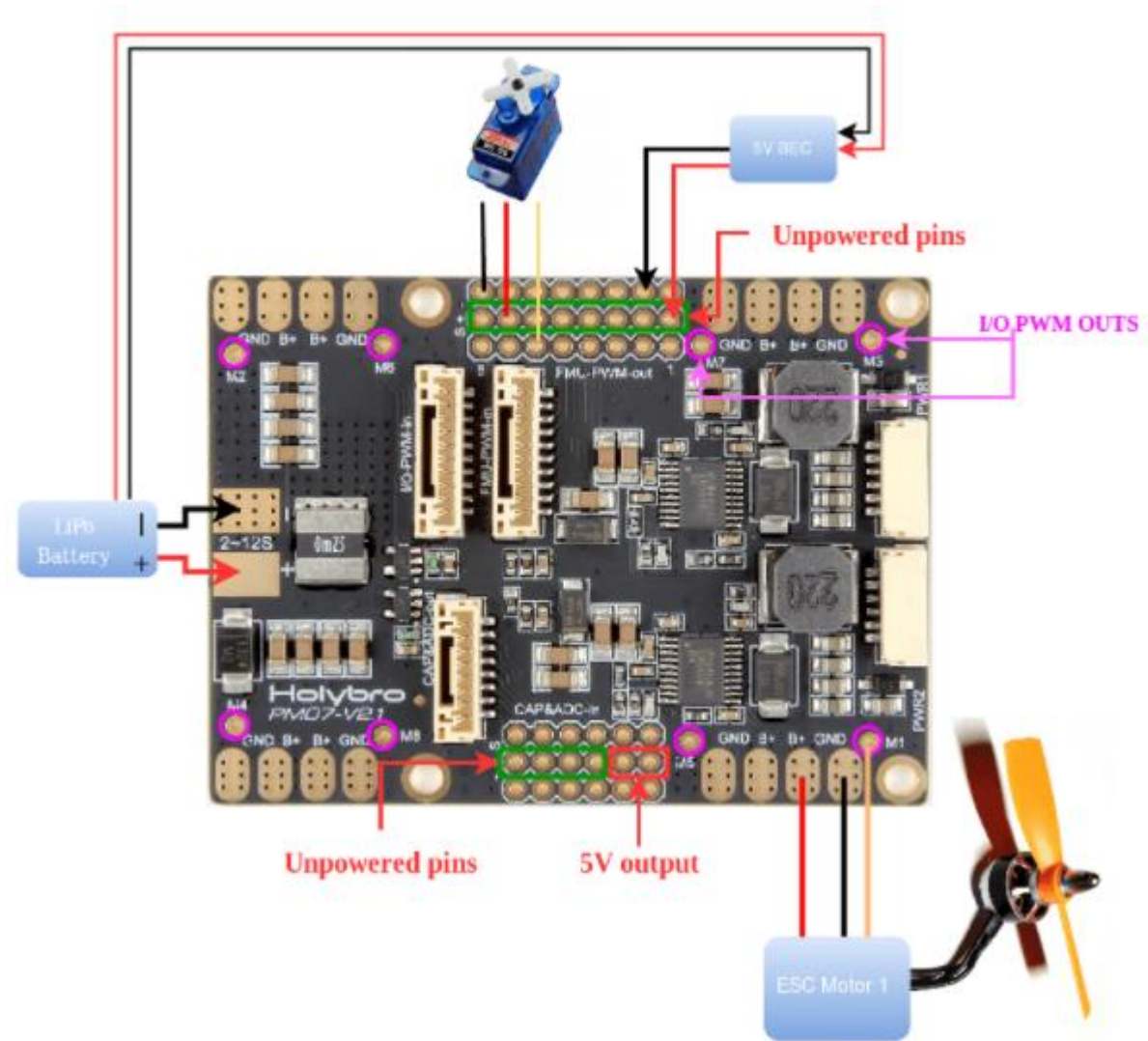


Figure 57: Example Wiring Diagram for Connecting a Servo and Motor to the PMB

The auxiliary pins of the Power Management Board are not internally powered. The rails need to be powered by a battery or through the BEC of an Electronic Stability Controller (ESC). The following table shows the necessary connections from the Pixhawk to the Power Management Board.

Table 6: Pixhawk to PMB Wiring Ports

Pixhawk 4	Power Management Board (PMB)
POWER1	POWER1
POWER2	POWER2
I/O PWM OUT	I/O PWM IN
FMU PWM OUT	FMU PWM IN

Along with the connections in Table 5, the receiver and GPS module must be connected to the Pixhawk as well. If correctly powered, the servo will move to its default position when connected to the auxiliary ports. To verify that the servo channel is set to the radio properly, open QGroundControl and go to the Flight Modes module. Toggle the switch assigned to the servo and ensure that the corresponding value changes. Next, open the parameter tab and search “RC_Map.” Find the corresponding port from the PMB and assign it to the same channel as the flight controller.

While attempting to test the model aircraft’s motor through QGroundControl, the team ran into an error. The motor output was not being recognized by the Pixhawk’s Power Management Board and QGroundControl. This meant we could not arm the aircraft to collect flight data or perform a flight test. Many troubleshooting solutions were attempted, including ones from both the Pixhawk website as well as hobby airplane forums about Pixhawks. In the end, it was decided that we would now be using Ardupilot Mission Planner instead of QGroundControl because of its history and reliability in comparison to QGroundControl.

3.4 Aerodynamic Performance Analysis

To understand the aerodynamic performance of both the full and sub-scales of the aircraft, a performance analysis of both was conducted.

3.4.1 Lift-Drag curves

The first analysis performed was creating the lift drag curves for the full and sub scale. This was done using Equations 3-5 The data used was gathered from aerodynamic and geometric analysis of the model, and similar aircraft.

$$C_L = \frac{W}{0.5SV^2\rho} \quad (3)$$

$$C_D = C_{D_o} + KC_L^2 \quad (4)$$

$$K = \frac{4}{3\pi e * AR} \quad (5)$$

The resulting Curves can be seen in Figure 58 and Figure 59.

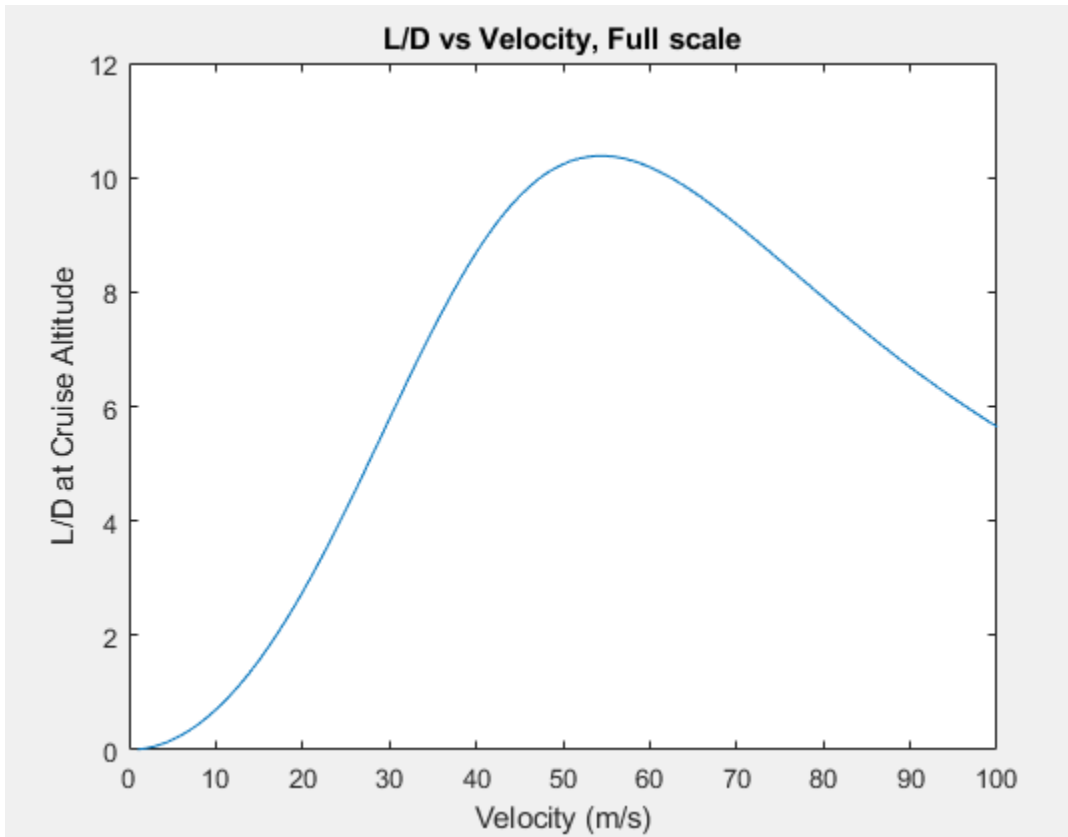


Figure 58: The L/D Curve of the Full Scale

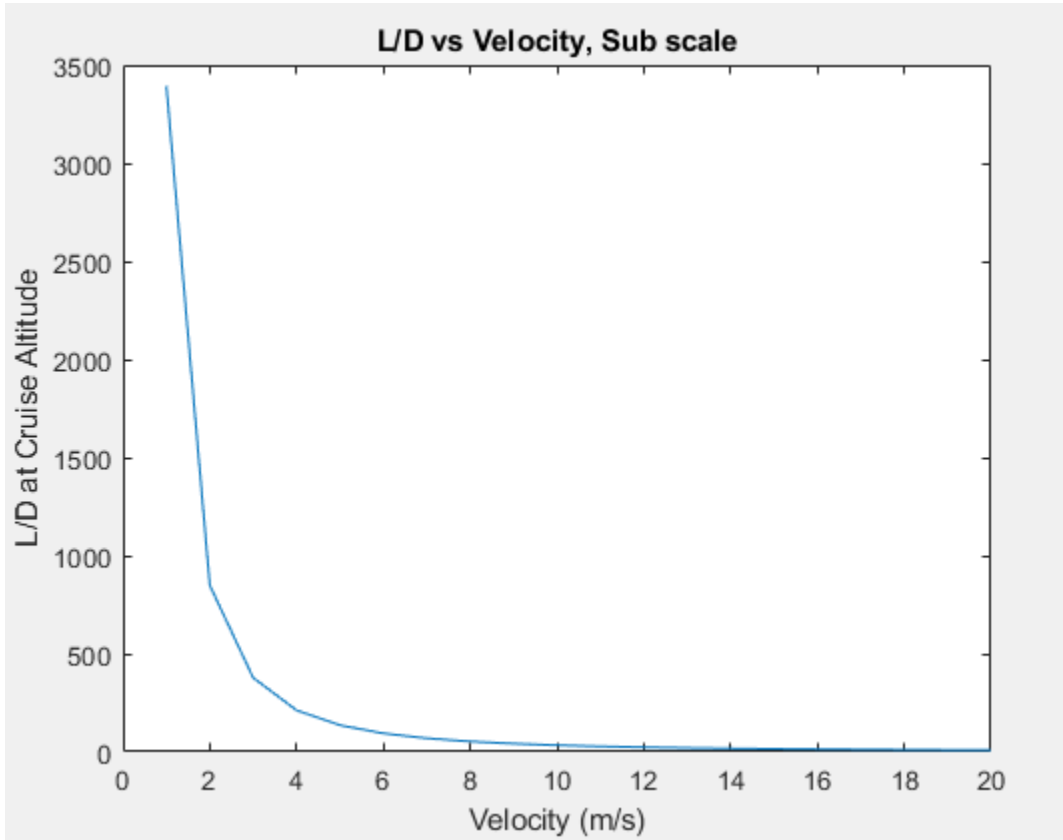


Figure 59: L/D Curve of the Sub Scale

These curves show the optimal velocity the aircraft should travel, where the full scale has a peak of 55 m/s, and the sub scale has a peak of 0 m/s and rapidly declines.

3.4.2 Required Velocity and Thrust

The next part of analysis performed was on the required velocity and thrust. This was done to understand at what speed each aircraft would stall at, as well as give an estimate of the thrust needed for the sub scale. To calculate the required velocity, equation 6 was used.

$$V = \sqrt{\frac{2W}{\rho S C_L}} \tag{6}$$

The stall velocity for the full scale was estimated to be 40.9 m/s, and the stall velocity for the sub-scale is 17.7 m/s. The next step was to estimate thrust needed to maintain cruise. Equation 7 shows the minimum required thrust for a given lift to drag ratio:

$$T = \frac{W}{\left(\frac{L}{D}\right)} \quad (7)$$

The required thrust for the full-scale is 942.3 newtons, and the required thrust for the sub scale is 1.5 newtons. These numbers are best estimations without the actual model built but give direction on how much power will be needed.

The thrust generated by the full-scale propeller engine was estimated at full throttle. The chosen engine for the full-scale was chosen to be a Lycoming O-360 engine that produces 120 kW of power. A propeller size of 1.93 m² was estimated as that is the size of propellers on similar aircraft. Equation X was used to calculate the thrust generated.

$$T_{propeller} = 2(EnginePower^2 \rho A)^{1/3} \quad (8)$$

The estimated maximum thrust of the full scale is 5830 N. This is assuming 100% propeller efficiency and maintaining cruise conditions.

3.4.3 Service Ceilings and Rate of Climb

The rate of climb is a useful piece of information to understand about the model and full scale. Equations 9-11 were used to find the rate of climb. Using the rate of climb, an iterative process was used to find the service ceiling of the full-scale using equations 9-11.

$$RC_{max} = \sqrt{\frac{\left(\frac{W}{S}\right)}{3\rho C_{D_0}}} \left(\frac{T}{W}\right)^{\frac{3}{2}} \left(1 - \frac{Z}{6} - \frac{3}{2\left(\frac{T}{W}\right)^2 \left(\frac{L}{D}\right)_{max}^2 (Z)}\right) \quad (9)$$

$$Z = 1 + \sqrt{1 + \frac{3}{\left(\frac{T}{W}\right)^2 \left(\frac{L}{D}\right)_{max}^2}} \quad (10)$$

$$T = \left(\frac{\rho}{\rho_{sl}}\right) T_{sl} \quad (11)$$

The service ceiling of the aircraft is defined as when the rate of climb reaches 0.5 m/s, and the absolute ceiling is defined as when that value reaches 0. The service ceiling of the full-scale is 14550m, and the absolute ceiling is 14900m. This is comparable to the service ceiling of the Cessna 172, which is 13000m. The maximum rate of climb for the full-scale is 33m/s.

The absolute and service ceilings of the sub-scale are irrelevant for this project, as the legal limit for remote controlled aircraft is 400 ft. The maximum rate of climb for the sub-scale is estimated to be 1.63 m/s.

3.4.4 Determining Model Payload Drop Location

A MATLAB script was created to calculate the distance before the target point that the payload needed to be dropped. The script featured a loop that calculates the drag force at each time instant, as the magnitude of that force changes with velocity. The script also plots the trajectory of the payload after dropping out of the aircraft. The way the script is set up allows for easy manipulation of the flight velocity, drop height, cross sectional area, and mass of the payload.

The team determined that the model airplane will drop payloads in the shape of cubes. This decision came from both the ease to manufacture as well as many payloads on full scale aircraft being similar shapes as well. The drag coefficient of 1.42 was a number researched and is what is used in the MATLAB simulation of the ballistic calculations [15]. The script can be found in the Appendix and the plot is shown in section 4.1.

4 Results

4.1 Numerical Simulation Results

4.1.1 Drop Location Simulation Results

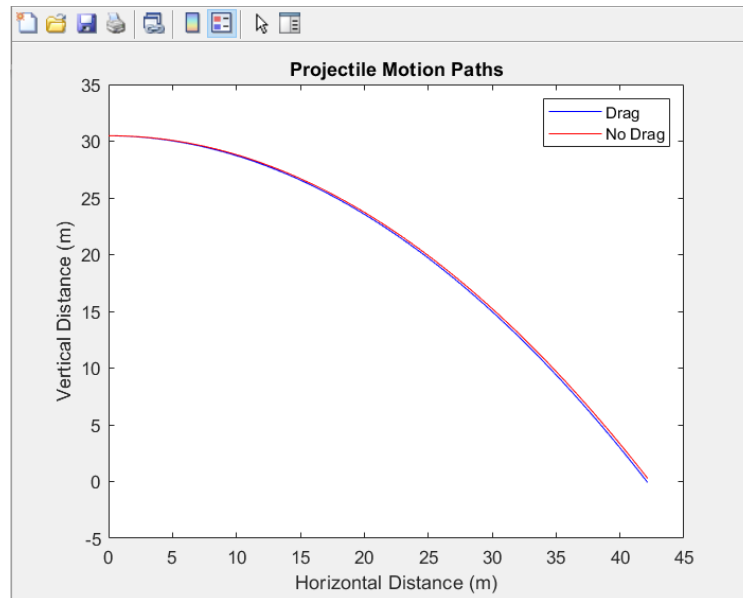


Figure 60: Projectile Motion Plot for Payload Drop

For a flight velocity of 17 meters per second and a flight altitude of 30.48 meters, the drop position is approximately 42.1577 meters before the target. The way the script is set up allows for easy manipulation of the flight velocity, drop height, cross sectional area, and mass of the payload.

4.2 Experimental Results

The final product weighed 1.9 kg. This is 0.78 kg lighter than the original estimation. It is important to note, however, that the final prototype did not include servos, the motor, and the payload and payload deployment mechanism. The estimates for the servos, motor, and payload/deployment system were 0.050, 0.231, and 0.275 kg respectively. Subtracting these from the original estimate yields a new estimate of 2.124 kg, still heavier than the measured weight.

Assuming all the missing components were present, it is not unreasonable to conclude that a fully functional prototype would have been underweight compared to predictions.

The first iteration of the glide test only contained a battery due to the rest of the electronics being inaccessible at the time due to extenuating circumstances. The aircraft was taken to Alden Hall at WPI to make use of the balcony. The plan was to launch the aircraft from the balcony into cloth bed sheets, held by groupmates and a few other kind volunteers. This test would be recorded from two different angles using cell phones. The purpose of this test, while we would get no numerical data due to the lack of electronics in it, was to see if the aircraft maintained a solid balanced flying posture, with no wobble or other extreme resulting scenarios. We conducted 3 of these tests. The first was launched at a flat angle of attack, it did well and remained steady throughout the glide. The second test had some human error involved. When it was launched, the tail of the aircraft hit the hand of the thrower, so it went into a steep nosedive quickly, but it remained stable throughout the flight. The third test had the aircraft thrown at a higher angle of attack. The aircraft handled it well, climbing for a bit and then heading back toward the ground. It remained aerodynamically stable throughout all three of the tests, demonstrating that the concept, design and construction of the aircraft was solid and successful.

The second iteration of the glide test was performed in the same environment as the first. The one major difference between the first and second iteration was the contents in the aircraft. This time, the battery, ESC, Pixhawk, telemetry module, airspeed sensor, and GPS module were all inside the fuselage of the aircraft. The plane flew similarly to the first iteration, gliding smoothly and being caught in a bedsheet below. With all the electronics being inside the aircraft, the team was able to calibrate the Pixhawk and collect in-flight data from the test. The telemetry log data from Mission Planner was converted into a .mat file for plotting purposes. The plots and MATLAB code used to create these plots are found in Appendix 2. The data is not totally what we expected. One reason this could have happened is the bandwidth limitations. Data was not being sent from the Pixhawk to Mission Planner fast enough, so some values may be inconsistent. . The roll rate was appeared to be negligible for the duration of the flight, meaning that the aircraft was stable.

5 Conclusions

The original plan of the project was to model both a full and sub scale model of our aircraft. Along with modeling a subscale aircraft, the goal was to build the subscale model and drop multiple payloads on a fully autonomous mission. The model is a 1:10 scale of the full-scale aircraft, where the total weight of the payloads for the full scale is 250 kg, and 250 g for the small scale. Both the full scale and the sub scale models were modeled. The modeling, manufacturing and electronics process of the subscale model took much longer than anticipated, causing time constraints when it came to the full flight test. The team was unable to achieve a full flight test, but glide tests were conducted to test the stability of the aircraft in unpowered flight. The objective of constructing a payload mechanism for the 1:10 scale aircraft was not achieved.

The team learned many lessons throughout the course of the project. This process of designing a full and sub scale prototype and then building the sub scale was completely new and uncharted territory for the entire team. It took a lot of trial and error to make progress on the project. The setbacks and failures that we faced in the progress were extremely beneficial, it taught us extremely valuable lessons. We learned the value of constant and concise communication among members of a project team. It was during the weeks when team meetings were not regularly held that individual understanding of progress/project goals seemed to deteriorate. The opposite effect was observed during the weeks that regular meetings were held: the entire team was on the same page and understood what had been done, what was being done, and what needed still to get done. The team also learned about the difference between CAD rendering and manufactured parts. Many of the parts that were 3D printed did not end up fitting properly or simply did not print correctly due to limitations of the machinery used. Tolerances for the various fits used on the prototype should have been considered, and parts should not have been designed solely with appearance in mind, but manufacturability as well. These lessons learned have led us to the belief that if we were to re-do the project again, we would complete the goals in a more efficient manner with greater success.

5.1 Recommendations for Future Work

For future follow-on work, priority should be given to the objective of this project that were unable to be achieved. The first recommendation would be to do a full flight test to calibrate

control surface servos and then attempt an autonomous mission. To do this, servos would need to be calibrated in Mission Planner as well as the motor. After calibration and planning a mission, the aircraft would be ready to take a test flight. The next step in the project would be to finalize a dropping mechanism and incorporate that into the aircraft. There is also potential for integrating an autonomous drop as well. The original plan was to manually drop the payload with a radio controller, but more research into Mission Planner's in-flight features may result in the ability to have the aircraft drop the payload autonomously at a waypoint. Developing takeoff/landing gear for the aircraft would be a good addition to help with flight testing. The system used in the project was not ideal because there was a high chance that the aircraft could break on any given test.

One simplification that was made during the construction process was taping the control surfaces to the wings. This decision was made so the team would be able to perform a glide test in time to record results. This simplification does not allow for the control surfaces on the wing to move. If the team was to do a full flight test, control surfaces would need to be connected on the front axis with the control horn and piano wire. This would involve reprinting the wing control surfaces to make the control surfaces straight and able to accept the carbon fiber spar as originally designed. Because of the limitations of 3D printing, it would be advisable to print the control horns as a separate piece in such a way that they could snap or slot into their respective control surfaces. The control surfaces themselves might also be better printed as separate pieces. To conduct a full flight test, the internals of the aircraft would have to be rewired as to be prepared for the servos and the motor because the current iteration of the wiring has it in a spot where attaching servos and motor would be extremely challenging.

In hindsight, the prototype would have been easier to work with if it had been constructed at a slightly larger scale (1:5 at most). Construction at a larger scale would have made it easier to fit electronics and a payload deployment mechanism inside the body, which proved to be a challenge over the course of the project. Another potential area for improvement is to replace the balsa wood that is currently being utilized for the ribs on the aircraft with a stronger plywood. The sturdier wood would be less likely to fracture and/or crack during assembly and flight.

Some pitfalls that our group encountered involved the planning process. The team often under-planned and sometimes overlooked details that seemed minor at the time but ended up shaping how the project came out. This stemmed from a general lack of background and skill in

designing and constructing remotely piloted aircraft. As a result, time and effort was spent investigating how to develop a prototype capable of flight that should have been spent designing and constructing a payload retention/deployment mechanism. In the beginning of the project, many ideas for building and designing the aircraft were tried and scrapped, causing a significant time loss. The most important thing for a team to consider in the future is planning what tasks need to get done and when they need to get done by. This will give the team direction of what should be focused and iterated on during any given time.

References

- [1] United States Army. (2015, March 27). *Force 2025 and Beyond*. www.army.mil. Retrieved November 28, 2021, from <https://www.army.mil/standto/archive/2015/03/27/>.
- [2] Van Straaten, N.,J. (2015). Autonomous aerial resupply systems needed in BCTs: Army logistician. *Army Sustainment*, 47(3), 5-6.
<http://ezproxy.wpi.edu/login?url=https://www.proquest.com/trade-journals/autonomous-aerial-resupply-systems-needed-bcts/docview/1682660864/se-2?accountid=29120>
- [3] Gouré, D. (2019, March 14). *From out of The skies: The revolution in precision airdrop delivery*. Retrieved April 13, 2022, from <https://www.lexingtoninstitute.org/from-out-of-the-skies-the-revolution-in-precision-airdrop-delivery/>
- [4] *Joint Precision Airdrop System (JPADS)*. USAASC. (n.d.). Retrieved April 13, 2022, from <https://asc.army.mil/web/portfolio-item/cs-css-joint-precision-airdrop-system-jpads/>
- [5] Benney, R., Barber, J., McGrath, J., McHugh, J., Noetscher, G., & Tavan, S. (2012). 18th AIAA Aerodynamic Decelerator Systems Technology Conference and Seminar. In *The Joint Precision Airdrop System Advanced Concept Technology Demonstration* . Natick, MA; US Army Research, Development and Engineering Command.
- [6] Omer Ozkan & Omer Atli (2021) Transporting COVID-19 testing specimens by routing unmanned aerial vehicles with range and payload constraints: the case of Istanbul, *Transportation Letters*, 13:5-6, 482-491, DOI: 10.1080/19427867.2021.1896063
- [7] Joshua, M., & Eaton, A. N. (2013). Point of impact: Delivering mission essential supplies to the warfighter through the joint precision airdrop system. In *Systems conference (SysCon)*.
- [8] Benney, R., Barber, J., McGrath, J., McHugh, J., Noetscher, G., & Tavan, S. (2005). The new military applications of precision airdrop systems. In *Infotech at aerospace*.

- [9] Henry, M. P. (2018). Autonomous transportation: Combat power in the 21st century: Army logistician. *Army Sustainment*, 50(6), 56-58.
- <http://ezproxy.wpi.edu/login?url=https://www.proquest.com/trade-journals/autonomous-transportation-combat-power-21st/docview/2136834771/se-2?accountid=29120>
- [10] Henry, M. P. (2018). Autonomous transportation: Combat power in the 21st century: Army logistician. *Army Sustainment*, 50(6), 56-58.
- <http://ezproxy.wpi.edu/login?url=https://www.proquest.com/trade-journals/autonomous-transportation-combat-power-21st/docview/2136834771/se-2?accountid=29120>
- [11] Li, Y., Yang, W., & Huang, B. (2020). Impact of UAV delivery on sustainability and costs under traffic restrictions. *Mathematical Problems in Engineering*, 2020, 1–15.
- <https://doi.org/10.1155/2020/9437605>
- [12] Ivanova, Ksenia, et al. “Automated and Autonomous Systems for Combat Service Support: Scoping Study and Technology Prioritisation.” *Australian Government Department of Defense Science and Technology*, Oct. 2016.
- [13] U.S. Army Joint Precision Airdrop System. <https://asc.army.mil/web/portfolio-item/cs-css-joint-precision-airdrop-system-jpads/>. Accessed Sep. 12, 2020.
- [14] National Society of Professional Engineers. *Code of Ethics for Engineers*. <https://www.nspe.org/sites/default/files/resources/pdfs/Ethics/CodeofEthics/NSPECodeofEthicsforEngineers.pdf>. Accessed Sep. 12, 2020.
- [15] Joyce, K., Ferrari, C., Warren, M., Debski, R., Schwend, W., Cooper, T., de Crespigny, T., & D'Attilio, S. (2021). Long Range Autonomous Aerial Delivery Systems.: Worcester Polytechnic Institute.
- [16] GnarlyDesign, & Instructables. (2017, October 26). Simple robot claw. Instructables. Retrieved April 17, 2022, from <https://www.instructables.com/Simple-Robot-Claw/>

6 Appendix

6.1 Appendix 1: Drop Location MATLAB Code

Table of Contents

.....	1
Sets up intial conditions	1
Starts a loop for Projectile Motion with Drag	1
Plots	25

```
clc; clear all; close all;

Vx = 17; %m/s sub scale speed
Vy = 0; %Drop initially has 0 y velocity
```

Sets up intial conditions

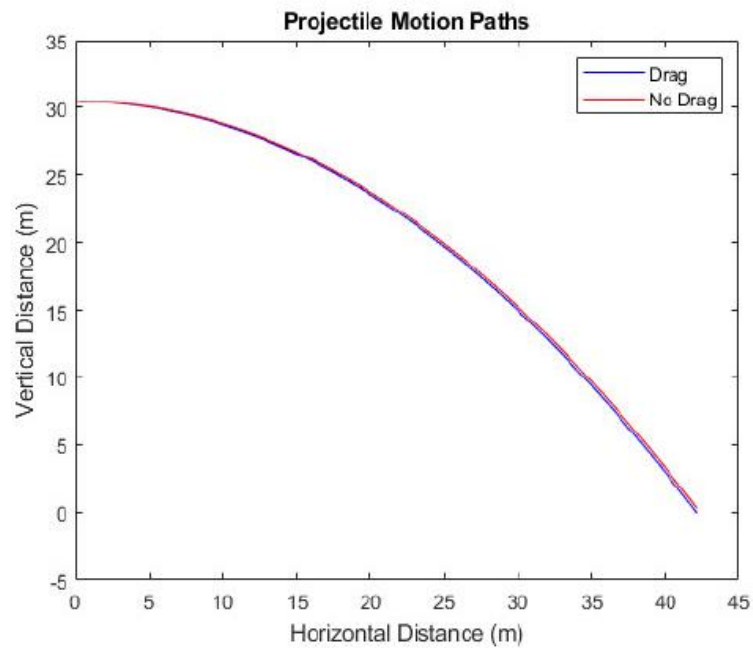
```
V = sqrt(Vx^2 + Vy^2); %Determines V by combining v of both axes
G = 9.80665; %m/s^2 Acceleration due to Gravity
CD = 1.05; %Drag coefficient
Area = 0.00129032; %m^2 cross section area of the payload
Mass = 0.25; %Kg mass of payload
x(1) = 0; %intial x postion
y(1) = 30.48; %intial y postion
xf(1) = 0; %intial xf postion
yf(1) = 30.48; %intial yf postion
rho = 1.2; %kg/m^3 Air Density @ Sea Level
D = rho*CD*Area/2; %constant needed for drag calculations
created
t(1) = 0; %sets intial time
dt = 0.01; %s set the intervals at which time will be
evaluated
i = 1; %sets counter/index
V_t = sqrt( (2*Mass*G)/(rho*Area*CD) );
```

Starts a loop for Projectile Motion with Drag

```
while min(y) > -0.01;
    t = t + dt;
    i = i + 1;
    xf(i) = xf(i-1) + Vx.*dt;
    yf(i) = yf(i-1) + Vy.*dt;
    AxD = - ( (D*Vx) / Mass );
    AyD = -G - ( (D*Vy) / Mass );
    Vx_new = Vx + AxD * dt;
    Vy_new = Vy + AyD * dt;
    x(i) = x(i-1) + Vx_new * dt + 0.5 * AxD * dt^2;
    y(i) = y(i-1) + Vy_new * dt + 0.5 * AyD * dt^2;
    Vx = Vx_new;
    Vy = Vy_new;
    Drop_Position = [-x(i)]
end;
```


Plots

```
plot(x,y,'b'), hold on;           %plots the Projectile Motion
    with Drag
plot(xf,yf,'r'), hold off;       %plots the Projectile Motion
    without Drag
xlabel('Horizontal Distance (m)'); %labels the x axis "Horizontal
    Distance (m)"
ylabel('Vertical Distance (m)');  %Labels the y axis "Vertical
    Distance (m)"
title('Projectile Motion Paths'); %Gives a Title "Projectile
    Motion Paths"
legend('Drag', 'No Drag')
```



Published with MATLAB® R2020a

6.2 Appendix 2: Glide Test Data MATLAB Code

Table of Contents

.....	1
Time Vectors	1
Yaw, Pitch, Roll and Speeds	1
X Acc, Gyro, Mag,	5
Y Acc, Gyro, Mag,	7
Z Acc, Gyro, Mag,	9

```
clc; clear all; close all;
load('2022-04-14 17-01-10.tlog.mat')
```

Time Vectors

```
t528 = length(roll_mavlink_attitude_t);
time1 = [1:1:t528];

t203 = length(zgyro_mavlink_scaled_imu2_t);
time2 = [1:1:t203];
```

Yaw, Pitch, Roll and Speeds

```
%Roll
figure(1)
plot(time1,roll_mavlink_attitude_t(:,2))
title('Glide Test Roll Angle')
xlabel('Time (ms)')
ylabel('Roll Angle, Deg')

%Rollspeed
figure(2)
plot(time1,rollspeed_mavlink_attitude_t(:,2))
title('Glide Test Roll Speed')
xlabel('Time (ms)')
ylabel('Roll Speed, Deg/Sec')

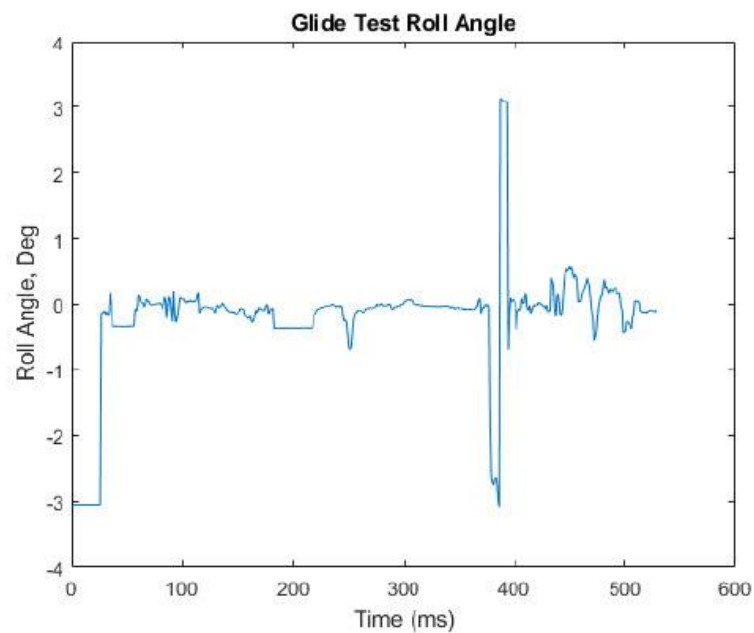
% Yaw
figure(3)
plot(time1,yaw_mavlink_attitude_t(:,2))
title('Glide Test Yaw Angle')
xlabel('Time (ms)')
ylabel('Yaw Angle, Deg')

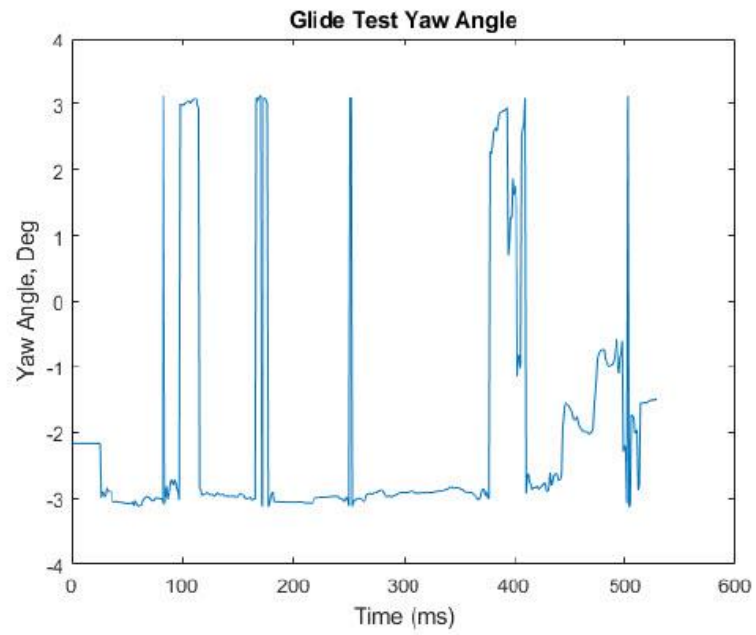
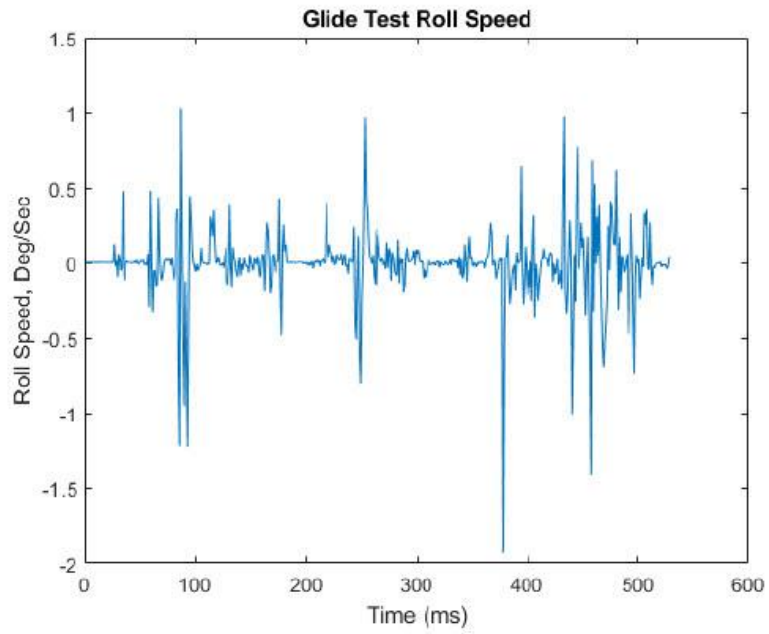
%Yawspeed
figure(4)
plot(time1,yawspeed_mavlink_attitude_t(:,2))
```

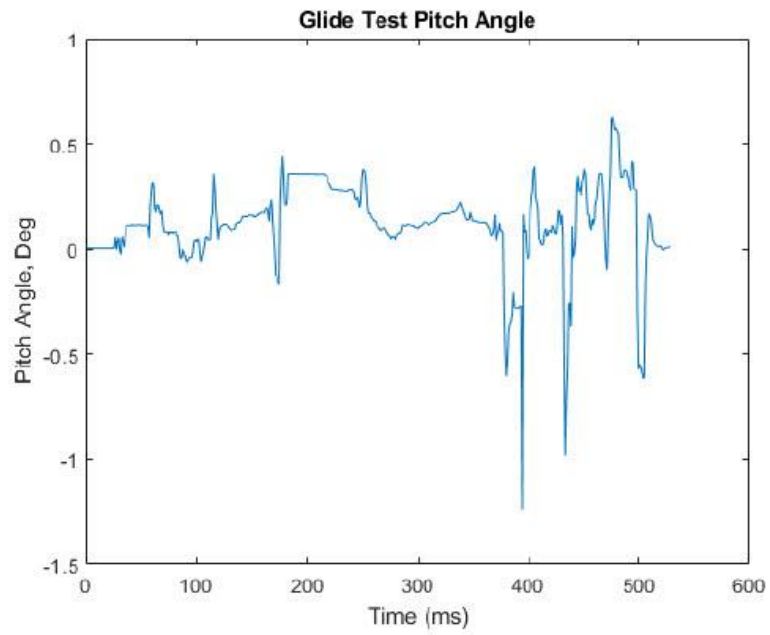
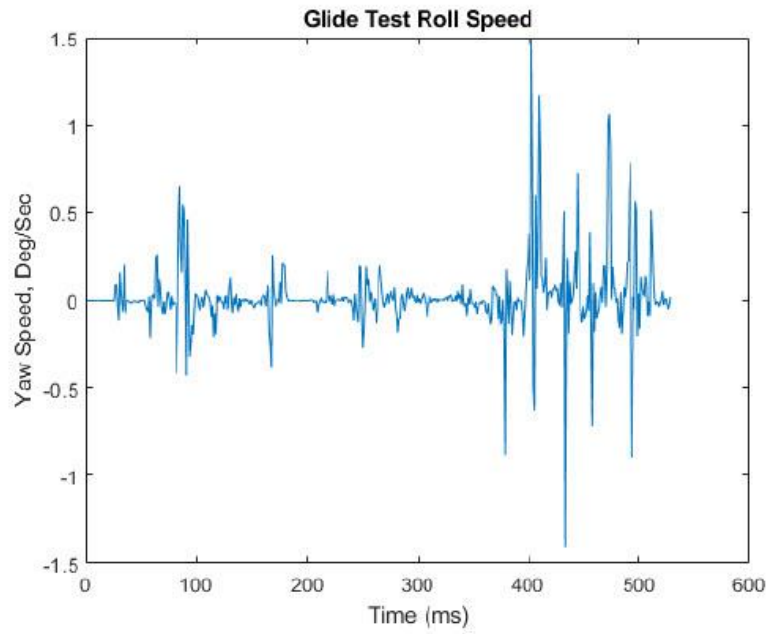
```
title('Glide Test Roll Speed')
xlabel('Time (ms)')
ylabel('Yaw Speed, Deg/Sec')
```

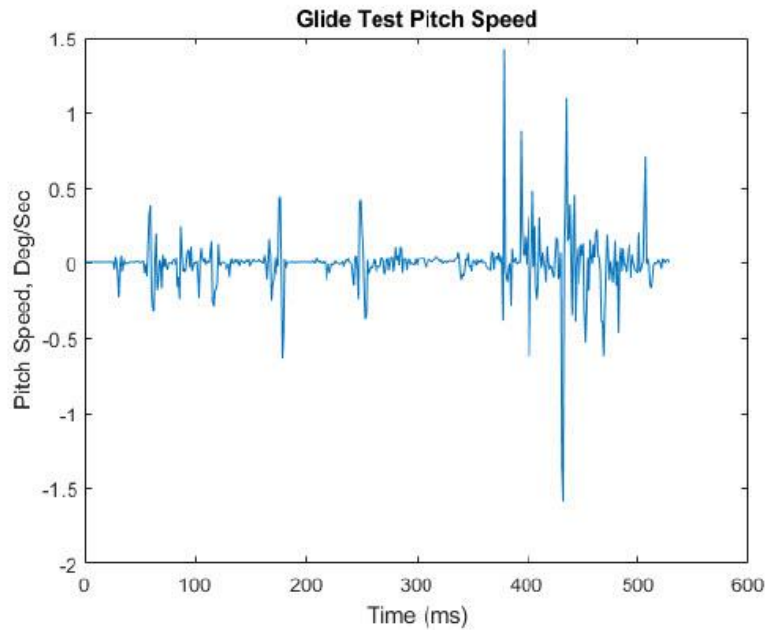
```
%Pitch
figure(5)
plot(time1, pitch_mavlink_attitude_t(:,2))
title('Glide Test Pitch Angle')
xlabel('Time (ms)')
ylabel('Pitch Angle, Deg')
```

```
%Pitch Speed
figure(6)
plot(time1, pitchspeed_mavlink_attitude_t(:,2))
title('Glide Test Pitch Speed')
xlabel('Time (ms)')
ylabel('Pitch Speed, Deg/Sec')
```









X Acc, Gyro, Mag,

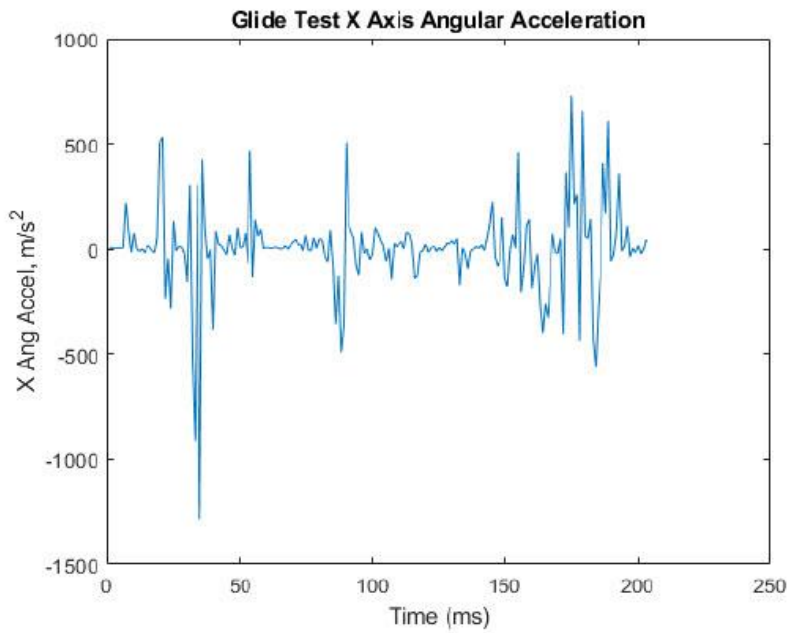
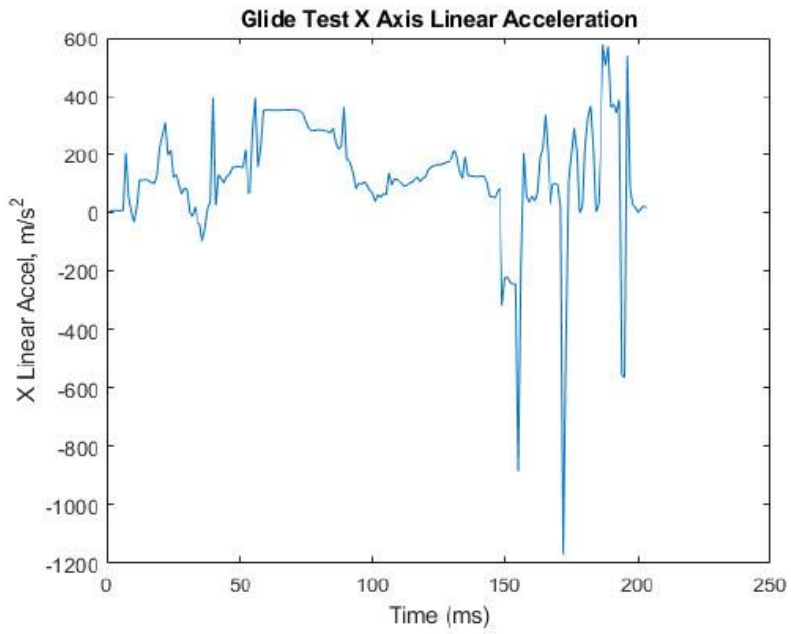
```

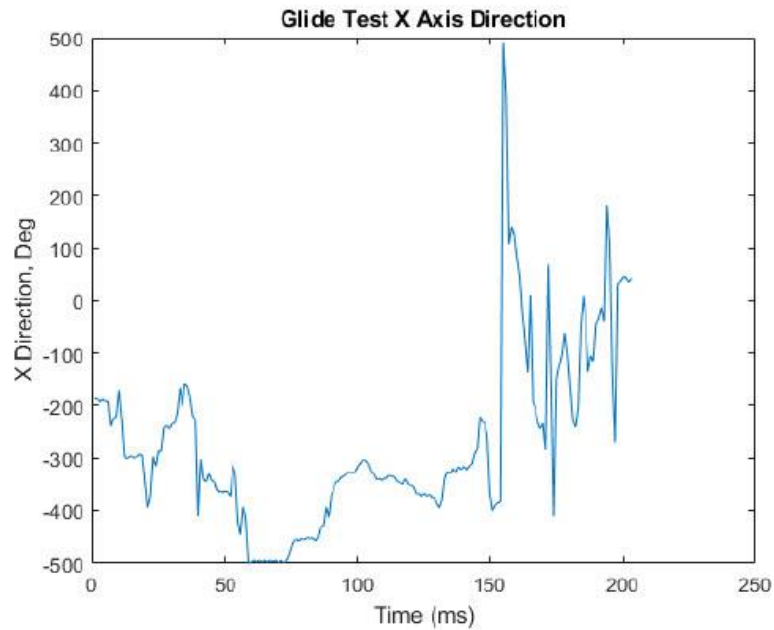
figure(7)
plot(time2, xacc_mavlink_scaled_imu2_t(:,2))
title('Glide Test X Axis Linear Acceleration')
xlabel('Time (ms)')
ylabel('X Linear Accel, m/s^2')

figure(8)
plot(time2, xgyro_mavlink_scaled_imu2_t(:,2))
title('Glide Test X Axis Angular Acceleration')
xlabel('Time (ms)')
ylabel('X Ang Accel, m/s^2')

figure(9)
plot(time2, xmag_mavlink_scaled_imu2_t(:,2))
title('Glide Test X Axis Direction')
xlabel('Time (ms)')
ylabel('X Direction, Deg')

```



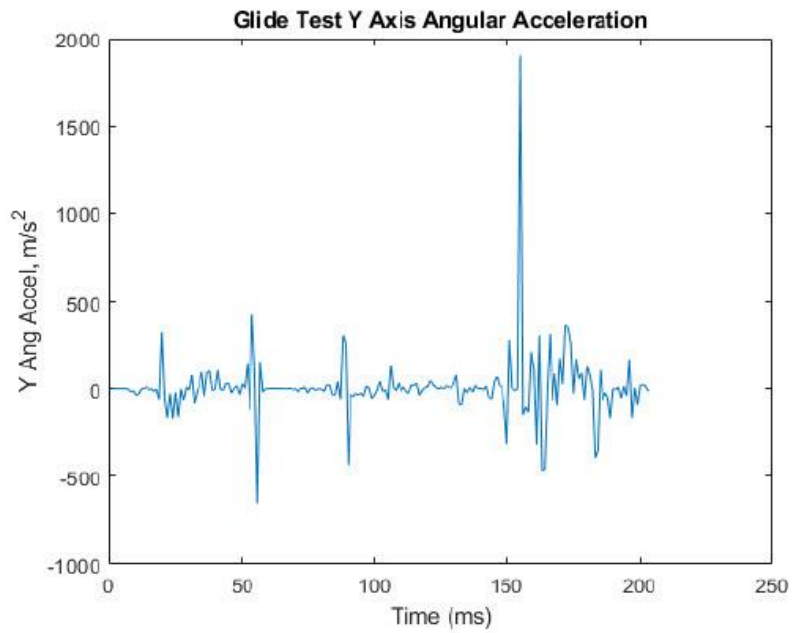
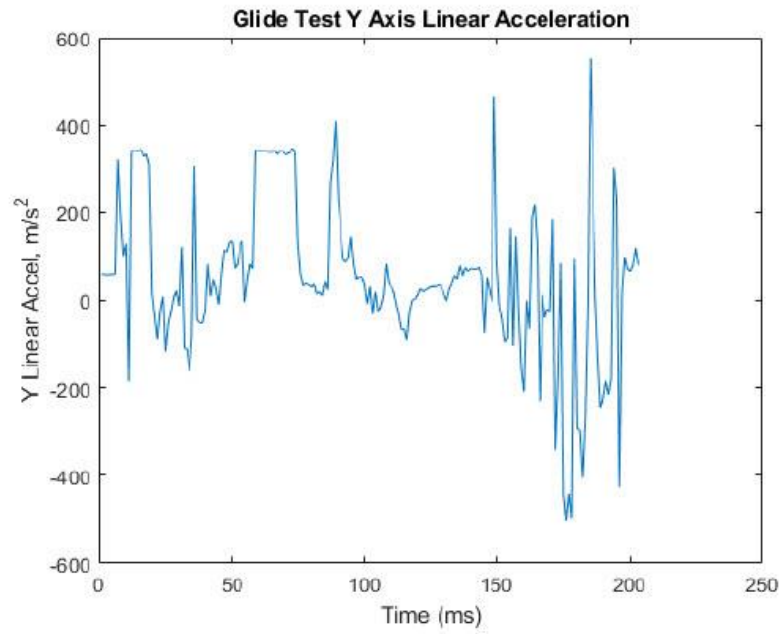


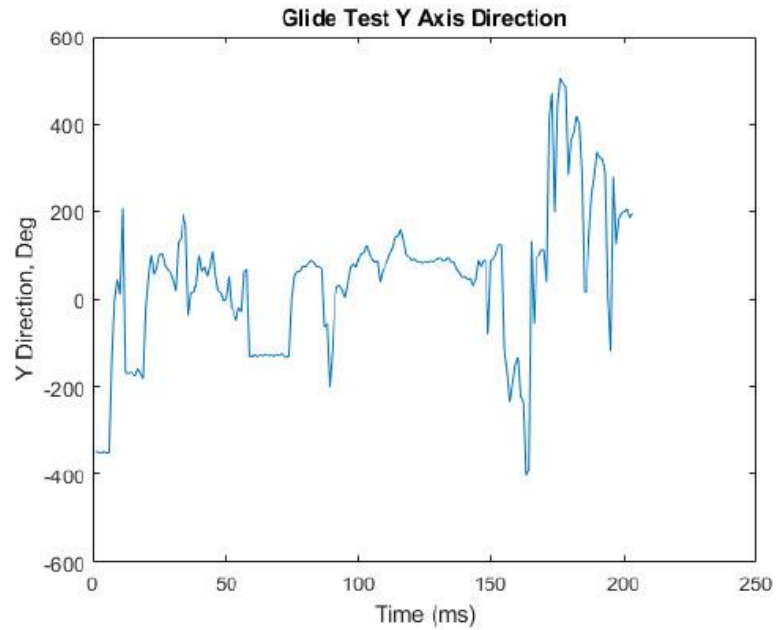
Y Acc, Gyro, Mag,

```
figure(10)
plot(time2, yacc_mavlink_scaled_imu2_t(:,2))
title('Glide Test Y Axis Linear Acceleration')
xlabel('Time (ms)')
ylabel('Y Linear Accel, m/s^2')

figure(11)
plot(time2, ygyro_mavlink_scaled_imu2_t(:,2))
title('Glide Test Y Axis Angular Acceleration')
xlabel('Time (ms)')
ylabel('Y Ang Accel, m/s^2')

figure(12)
plot(time2, ymag_mavlink_scaled_imu2_t(:,2))
title('Glide Test Y Axis Direction')
xlabel('Time (ms)')
ylabel('Y Direction, Deg')
```



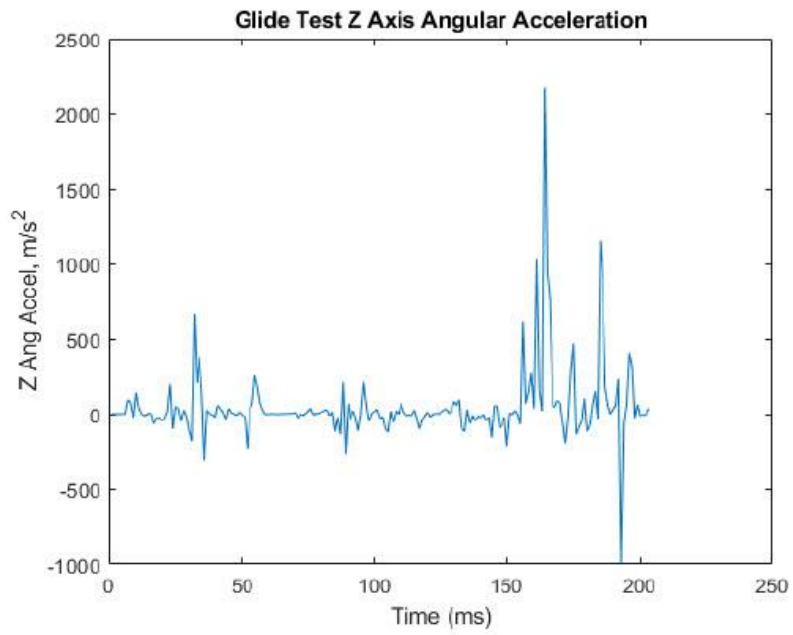
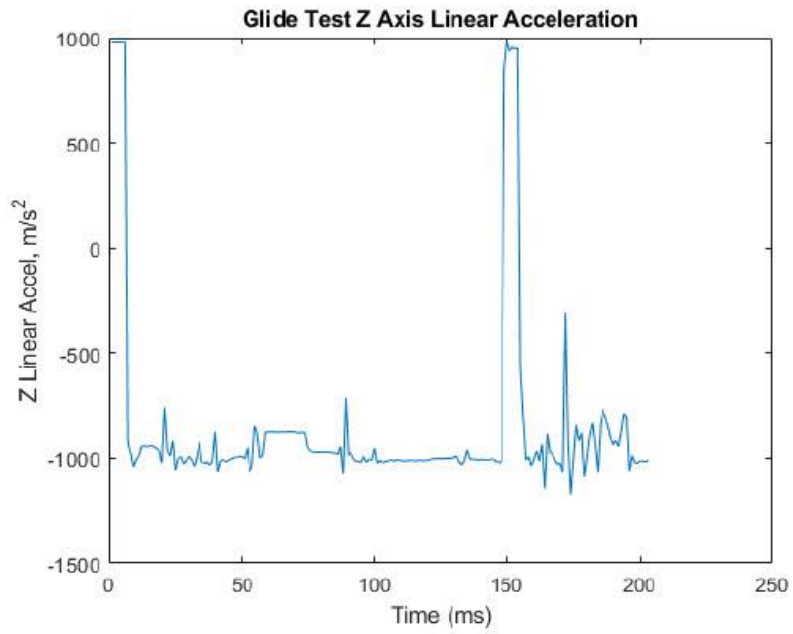


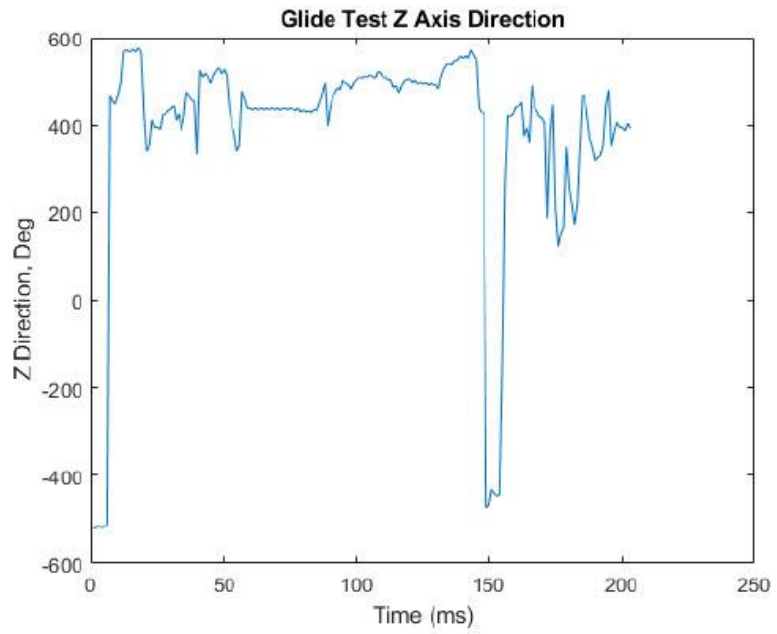
Z Acc, Gyro, Mag,

```
figure(13)
plot(time2, zacc_mavlink_scaled_imu2_t(:,2))
title('Glide Test Z Axis Linear Acceleration')
xlabel('Time (ms)')
ylabel('Z Linear Accel, m/s^2')
```

```
figure(14)
plot(time2, zgyro_mavlink_scaled_imu2_t(:,2))
title('Glide Test Z Axis Angular Acceleration')
xlabel('Time (ms)')
ylabel('Z Ang Accel, m/s^2')
```

```
figure(15)
plot(time2, zmag_mavlink_scaled_imu2_t(:,2))
title('Glide Test Z Axis Direction')
xlabel('Time (ms)')
ylabel('Z Direction, Deg')
```



Published with MATLAB® R2020a

6.3 Appendix 3: L/D Curves MATLAB Code

```
clc; clear all; close all;

%aerodynamic constants
C_L0 = 0.5079;
C_Lalpha = 3.1589;
C_La = C_Lalpha;
C_D0 = 0.0289;
K = 0.0803;
C_Lmax = 1.0592;

CL_full = 0.51;
Cd_full = C_D0 + K*CL_full^2;

%full scale
weight_full = 1000;
S_full = 15;
rho_full = 0.7364;

%sub scale
weight_sub = 2;
S_sub = .15;
rho_sub = 1.225;

%create L/d curve and plot

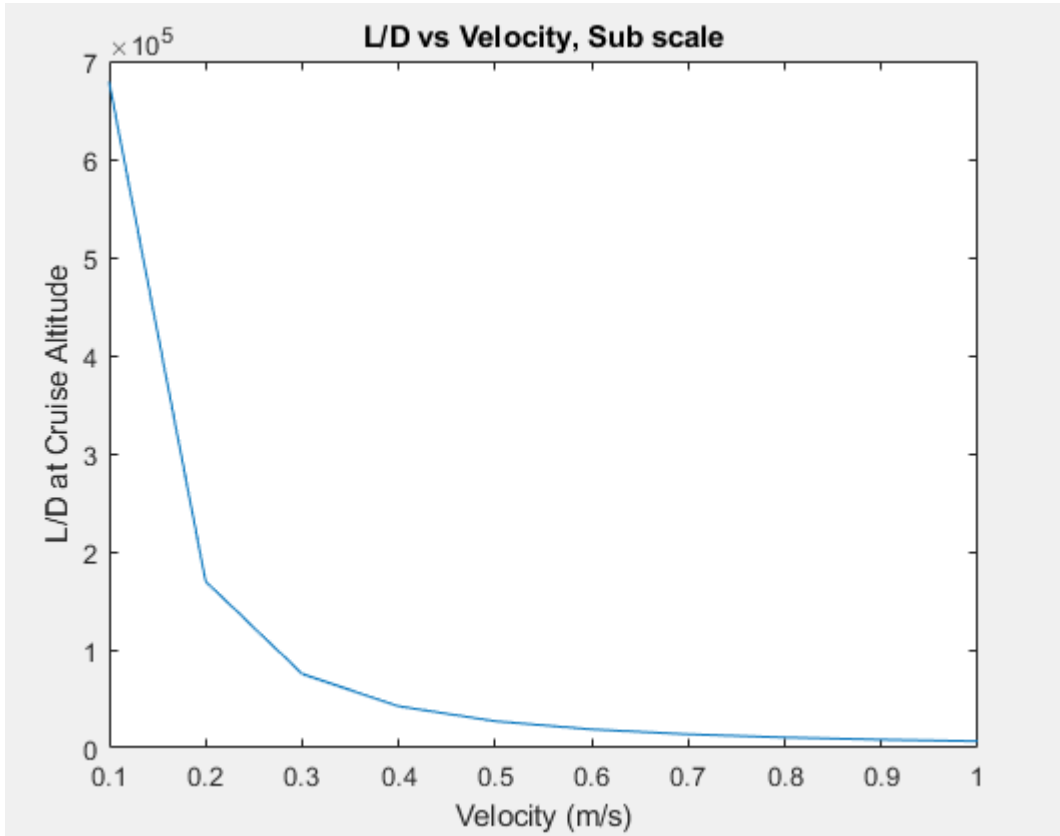
for V = 1:100
    CL_full_worst = (weight_full)*9.8/(.5*rho_full*V^2*S_full);
    Cd_full_worst = C_D0 + K*CL_full_worst^2;
    Ld_full(V) = CL_full_worst/Cd_full_worst;
    V_plot(V) = V;
    V=V+1;
end

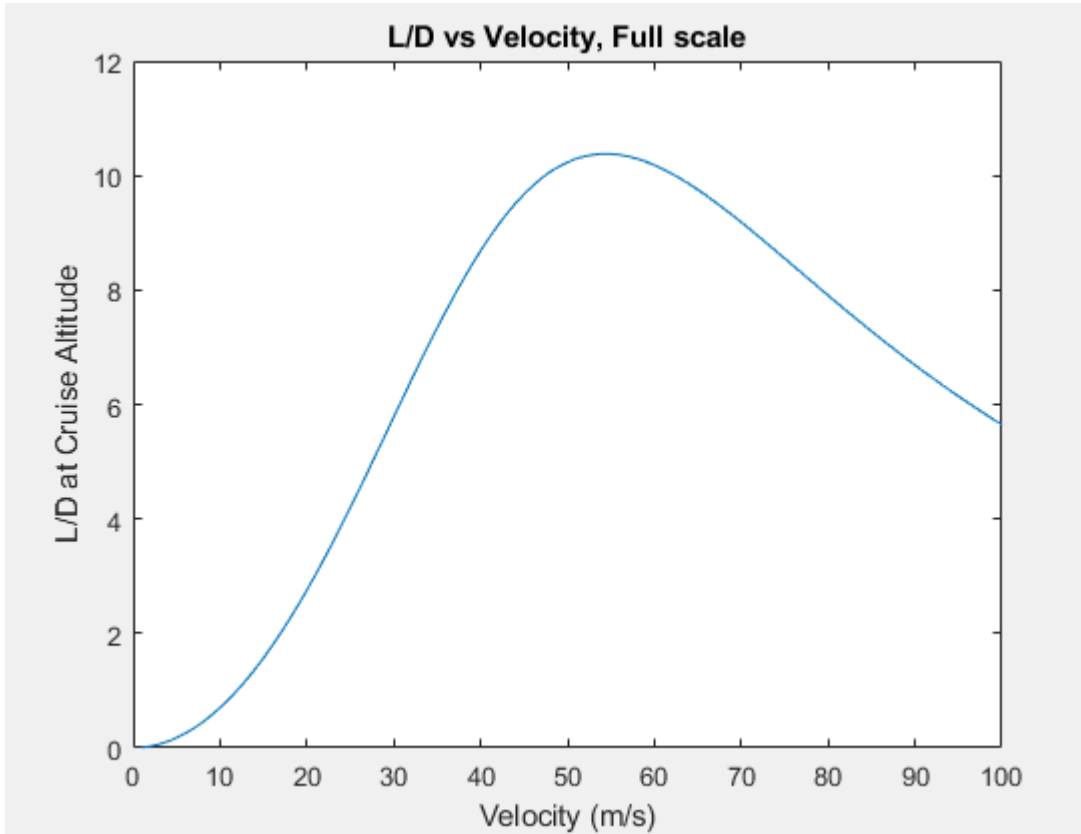
figure (1)
plot(V_plot,Ld_full)
title('L/D vs Velocity, Full scale')
xlabel('Velocity (m/s)')
ylabel('L/D at Cruise Altitude')

for v = 1:10
    vsub(v) = v/10;
    CL_sub_worst = (weight_sub)*9.8/(.5*rho_sub*vsub(v)^2*S_sub);
    Cd_sub_worst = C_D0 + K*CL_sub_worst^2;
    Ld_sub(v) = CL_sub_worst/Cd_full_worst;
    v_plot(v) = vsub(v);

    v=v+1;
end
figure (2)
```

```
plot(v_plot,Ld_sub)
title('L/D vs Velocity, Sub scale')
xlabel('Velocity (m/s)')
ylabel('L/D at Cruise Altitude')
```





6.4 Appendix 4: Rate of Turn MATLAB Code

```

clc; clear all; close all;

%constants and vairables
CL_max = 1.05;
W = 2*9.8;
rho = 1.225;
C_D0 = 0.0289;
S = .15;
K = 0.0803;
V = 17;

Tmax = 20;

%calculations
Q = .5*rho*(V^2);
n_max_alpha = (Q*CL_max)/(W/S);
n_max_t = ((Q/((K*W)/S))*((Tmax/W)-((Q*C_D0)/(W/S))))^0.5;

nmax_all = [n_max_alpha; n_max_t];

nmax =min(nmax_all);

```

```
Rmin = (V^2)/(9.81*((nmax^2)-1)^.5));
```

6.5 Appendix 5: Rate of climb MATLAB Code

```
clc; clear all;

%constants
Tsea = 2;
rho = .7500;
rho_sea = 1.225;
C_D0 = 0.0289;
S = .15;
LDmax = 10.4;
W = 9.8 * 1;

%equations
T = (rho/rho_sea)*Tsea;
Z = 1 + sqrt(1+(3/((LDmax^2)*((T/W)^2))));
RC = sqrt(((W/S)*Z)/(3*rho*C_D0))*((T/W)^(3/2))*(1-(Z/6)-
(3/(2*((T/W)^2)*(LDmax^2)*Z)))
```

6.6 Appendix 6: Air Density from Altitude MATLAB Code

```
%h is altitude
h = 10000;
rhosl = 1.225;
tsl = 288.16;
if h < 11000

    th = tsl + ((-6.5*10^(-3))*h);
    rho = rhosl*(th/tsl)
end

if h >= 11000
    rho11 = 0.3642;
    rhoh=rho11*exp((-9.8*(h-11000))/(287*216.66))
end
```